MECHANISMS OF LASER-SURFACE INTERACTIONS

By

J. F. Ready

E. Bernal G.

SEMI-ANNUAL REPORT

To

Ballistic Research Laboratories

Contract No. DA-18-001-AMC-1040(X)

December 1966

Presented by

Honeywell Inc.

CORPORATE RESEARCH CENTER

Hopkins, Minnesota

MECHANISMS OF LASER-SURFACE INTERACTIONS

By

J. F. Ready

E. Bernal G.

SEMI-ANNUAL REPORT

To

Ballistic Research Laboratories

Contract No. DA-18-001-AMC-1040(X)

December 1966

Presented by

Honeywell Inc.

CORPORATE RESEARCH CENTER

Hopkins, Minnesota

ABSTRACT

This report extends earlier measurements on particle emission produced when approximately 50 megawatts/cm^2 pulses of radiation from a Q-switched ruby laser are absorbed at metal surfaces. Ion emission from carbon targets includes $(Li^6)^+$, $(Li^7)^+$, C^+, CH_3^+, H_2O^+, Na^+, and K^+ ions with energies up to 540 ev. Emission from single crystalline nickel targets includes ion species not observed before in this work, i.e., Na^{++} and H_2^+. Work using a quadrupole mass spectrometer to study neutral molecule emission has also been extended to carbon targets, which yield results similar to other target materials, and additional confirming work on the presence of high energy neutral molecules has been performed. Equipment under construction for measurement of the angular distribution of the ion emission is described. The expansion of the laser produced gas and resulting particle fluxes at a distance from the surface are discussed.

TABLE OF CONTENTS

LIST OF ILLUSTRATIONS

LIST OF ILLUSTRATIONS

SECTION I

INTRODUCTION

In previous reports [1, 2, 3] we have described measurements on particle emission produced in laser-surface interactions. The time-of-flight spectrometer used to measure ion emission and the quadrupole spectrometer used to measure neutral molecule emission were discussed. The emission produced by absorption of ruby laser radiation with a power density of 50 megawatts/cm^2 in 30 nanosecond pulses was studied for various target materials, particularly tungsten. The ions were found to be mainly alkali metals with energies up to several hundred electron volts, while the neutral molecule emission consisted of thermally desorbed gases such as H_2, CO, and CO_2, along with pulses of high energy neutral molecules having energies of the order of 100 ev.

In this report we describe extensions of these measurements. The work discussed here does not involve new types of measurements, but rather the use of different types of target materials. The results described here confirm results reported earlier. The general features of the emission from various types of target material are broadly similar, although there are persistent and important differences. Since the main features have been described previously[1, 2, 3], this report tends to dwell on and emphasize the differences.

However, the main interest in this contract work is in phenomena, rather than in differences between materials. Accordingly, since many of the phenomena which the present spectrometers can measure have now been relatively thoroughly studied, we are constructing equipment designed for different types of measurement. This equipment is described in Section IV.

Section II of this report deals with the work performed on ion emission, with emphasis on carbon and nickel targets. Section III discusses neutral gas emission and high energy neutral molecule emission from carbon, nickel, and titanium targets. Section III also devotes considerable space to a discussion of a rechecking and reconfirmation of earlier conclusions on high energy neutral molecules. This rechecking was necessitated by some apparently anomalous results obtained with titanium. These results were traced to inadequate control over spectrometer condition, but our earlier interpretations were confirmed and the influence of spectrometer condition is now more fully understood.

Section IV describes the new equipment and Section V is devoted to interpretative aspects, with emphasis on a treatment of the expansion of a laser produced gas cloud.

SECTION II

ION EMISSION

The ion emission from the surfaces of two new materials, nickel and carbon, has been studied. The sparking problems encountered in trying to extend ion emission measurements to higher flux densities have been identified.

The ion emission from single crystal nickel shows a composition that can be changed by flushing the spectrometer with hydrogen. Data from nickel also shows the first evidence of Na^{++} and H_2^+ in the ion spectrum. The emission from pyrolytic graphite contains sodium ions with initial energies in excess of 540 ev; these are the highest energies observed in our experiments.

A. ION EMISSION FROM CARBON

Two types of carbon targets were used in the time-of-flight (TOF) spectrometer. The first was machined from a piece of polycrystalline graphite stock and heated in air to a temperature of about 700°C to drive out organic contaminants. The second target was a piece of solid pyrolytic graphite[4].

Figure II-1 is a typical spectrum obtained upon irradiation of the polycrystalline graphite target with the unfocused output of a 5 megawatt laser pulse It contains pulses corresponding to singly ionized species of mass 6, 7, 12, 15, 18, 23, and 39. The two pulses corresponding to masses 6 and 7 have been identified as the two lithium isotopes; the other peaks correspond to C^+, CH_3^+, H_2O^+, Na^+ and K^+ respectively. We had previously observed the $(Li^7)^+$ peak from the other surfaces such as tungsten, but its height was much smaller than those of Na^+ or K^+. For stock graphite the $(Li^7)^+$ peak is comparable in magnitude to the other two alkali metals. The peak at mass 6

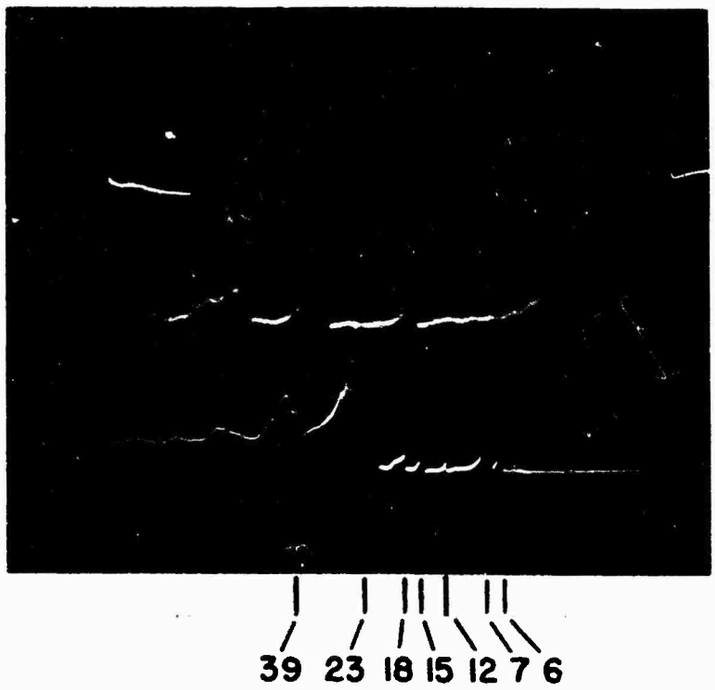

Figure II-1 - Ion Spectrum from polycrystalline graphite in TOF Spectrometer. Time increases from right to left. Lower trace starts with laser pulse (2μs/cm, .1 volt/cm). Upper trace is an expanded portion of the lower trace triggered by the mass 6 pulse (.5μs/cm, .05 volt/cm). The spectrometer potentials are: V = +2000 volts; V' = 0 volt.

was positively identified as being the $(Li^6)^+$ isotope for the following reasons: first, the ratio R(7/6) of the number of ions measured by integration of the areas of the 6 and 7 peaks is R(7/6) = 10.5, which is in good agreement with the accepted ratio [5] of 12.5 for the relative abundances of the two isotopes; second, if the peak were due to $(C^{12})^{++}$ one would expect a larger peak at $(C^{12})^+$ which it can be seen, is not the case; third, Figure II-2 shows a spectrum in which the $(C^{12})^+$ peak was enhanced by focusing the 5 megawatt laser pulse onto the target with a 330 mm. focal length lens, thereby evaporating more of the substrate. A comparison of Figures II-1 and II-2 clearly indicates that the relative heights of the 6 and 7 peaks remain fixed, while the ratio of 12 to 6 has increased, contrary to what one would expect if they were $(C^{12})^+$ and $(C^{12})^{++}$.

Figure II-2 also shows some peaks that are not found in Figure II-1 at masses 1, 13, 14, 15, which correspond to H^+, CH^+, CH_2^+, CH_3^+. Ion energies have not yet been measured for the polycrystalline graphite target.

The ion spectrum from pyrolytic graphite is different from the other surfaces studied previously both in the number of different masses found as well as their energies. This can be clearly seen in the three spectra shown in Figures II-3, II-4, and II-5. The first spectrum was obtained with no decelerating potential and shows a rather clean surface for which the only distinguishable peaks correspond to the three alkali metals Li^+, Na^+ and K^+. One can also see a rather large continuous background which may be caused by neutrals. The second spectrum was taken with a decelerating potential of 360 ev and it shows clearly two peaks corresponding to Na^+ and K^+. The third spectrum, Figure II-5, is for a decelerating potential of 540 v and it clearly shows that some of the sodium ions from pyrolytic graphite have initial energies in excess of 540 ev; such energies are more than twice as large as the ion energies measured previously from surfaces such as tungsten and platinum.

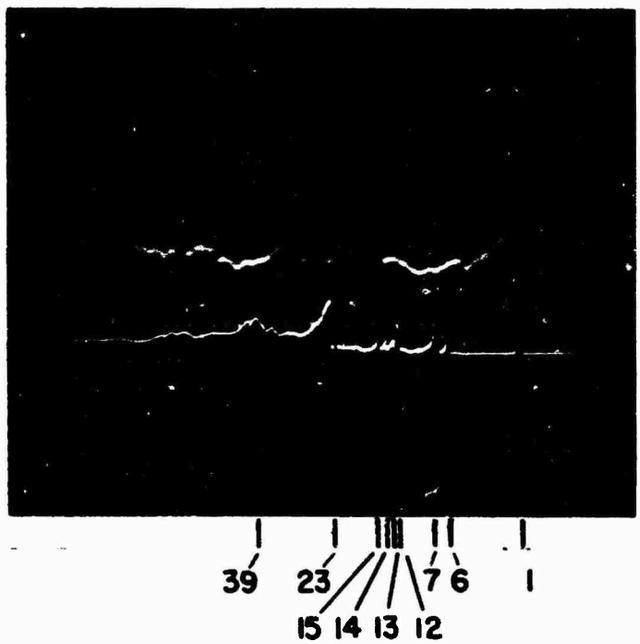

Figure II-2 - Ion spectrum from polycrystalline graphite. Same as Figure II-1 except that the flux density at the target has been increased by focusing with a 330 mm. focal length lens. The $(C^{12})^+$ peak is enhanced by the increased evaporation of substrate. Sensitivity of lower trace is .2 volt/cm.

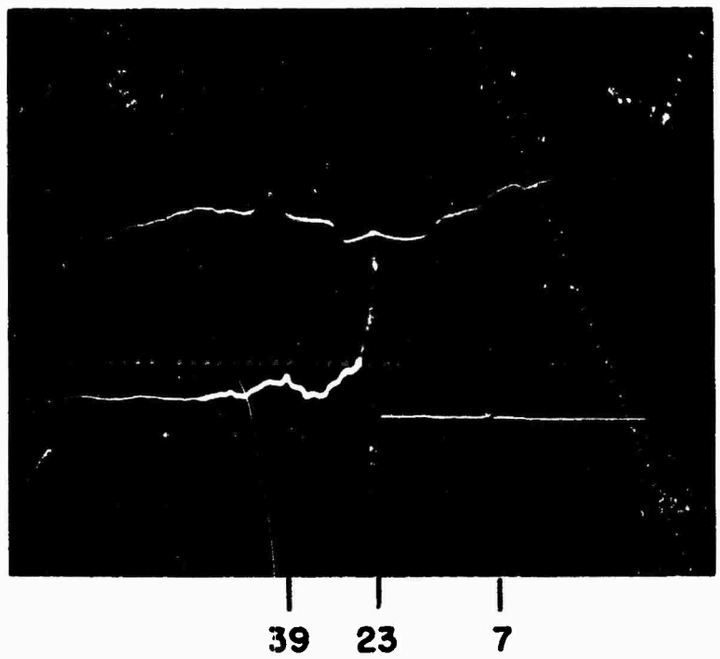

Figure II-3 - Ion spectrum from pyrolytic graphite in TOF spectrometer. Time increases from right to left. Lower trace starts with laser pulse (2μs/cm, .2 volt/cm). Upper trace is an expanded portion of the lower trace triggered by the mass 23 pulse (.5μs/cm, .05 volt/cm). The spectrometer potentials are: V = +2000 volts; V' = +2000 volts, i.e. zero decelerating potential.

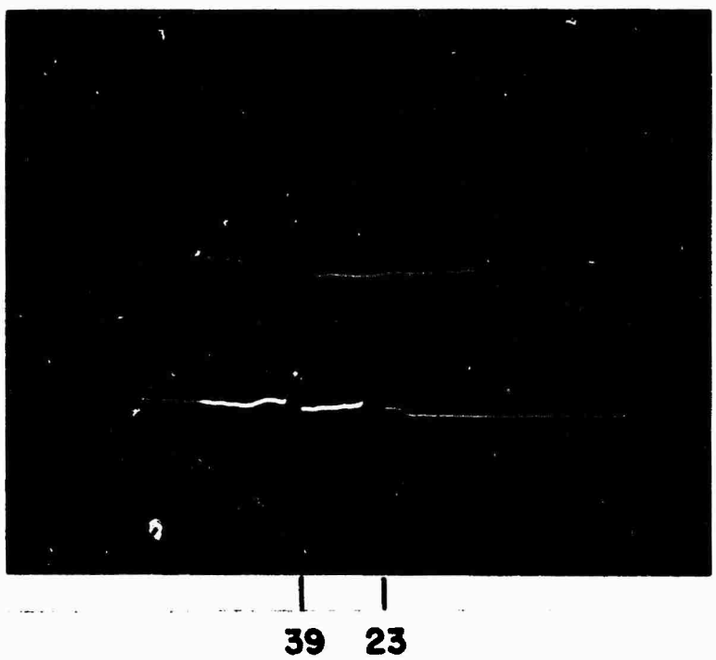

Figure II-4 - Ion spectrum from pyrolytic graphite in TOF spectrometer. All parameters are identical to those of Figure II-3 except V' = +2360 volts, i.e., 360 volts decelerating potential.

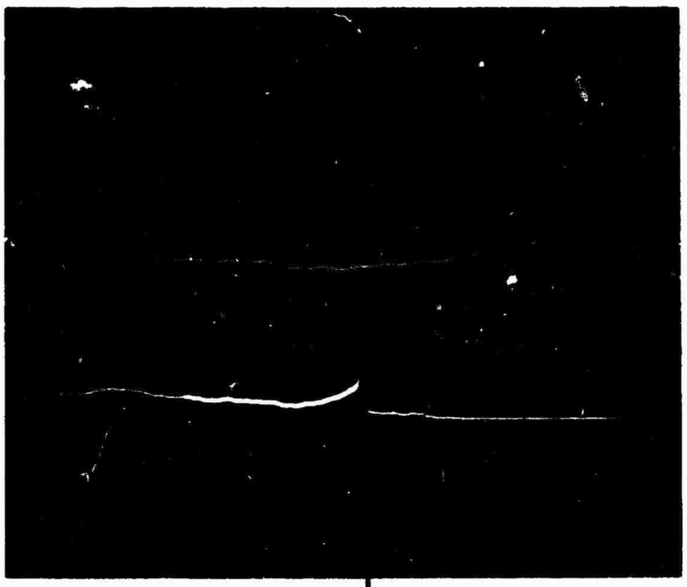

Figure II-5 - Ion spectrum from pyrolytic graphite. Same as Figure II-4 except V' = +2540 volts, i. e., 540 volts decelerating potential.

B. ION EMISSION FROM NICKEL

The ion emission from the (100) face of single crystal nickel was investig[illegible]. Interest in nickel was a result of reports that the (100) face could be covered with a monolayer of hydrogen, to the exclusion of all other adsorbed species[6, 7]. Such a property would have greatly simplified the task of understanding the mechanism for ion acceleration and would have eliminated any ambiguity in the interpretation of data from a non-mass discriminating instrument such as the one being built for angular distribution measurements.

The procedure used to study the nickel was to place two single crystal slabs in the TOF spectrometer and evacuate the instrument to a pressure of 4×10^{-8} Torr. Using the output of a Q-switched ruby laser in the range of 20-70 megawatts/cm^2, the slabs were irradiated on the (100) faces and the masses and energies of the ions produced were measured. Having determined the composition of the initial coverage on the nickel surface, the spectrometer was backfilled with hydrogen to a pressure of 1×10^{-4} Torr and held at that pressure while the target was irradiated with twenty pulses from the same ruby laser operating in the normal pulse mode and delivering about 1 joule per pulse. The irradiation with the millisecond-long pulses was used to heat the target for longer intervals of time than would be achievable with the Q-switched pulse in order to clean the surface of contaminants and encourage the adsorption of hydrogen. Next, the hydrogen was turned off, the spectrometer was pumped down to 7×10^{-8} Torr and the target irradiated with the Q-switched laser to look at the ion emission.

Typical spectra obtained before and after the attempt to cover the surface with hydrogen are shown in Figures II-6a and II-6b. The most obvious difference in the two spectra is the presence of hydrogen in b and its absence in a. In fact, before leaking hydrogen into the system and even after leaking it in to a pressure of 10^{-6} Torr, that species was only recorded occasionally

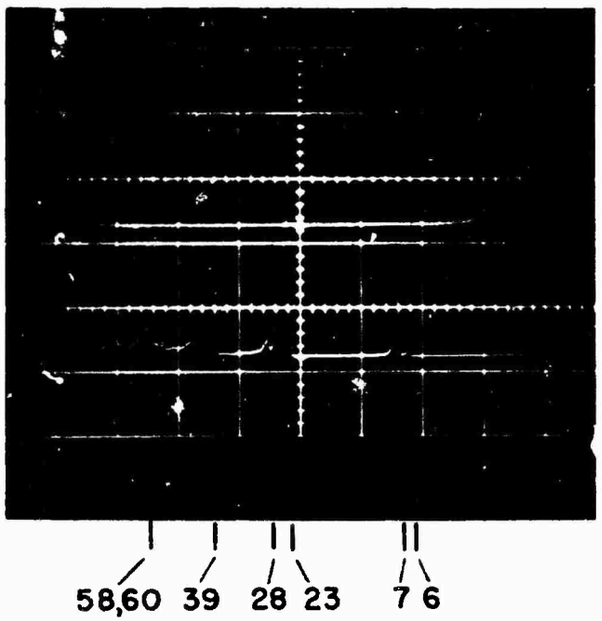

6a

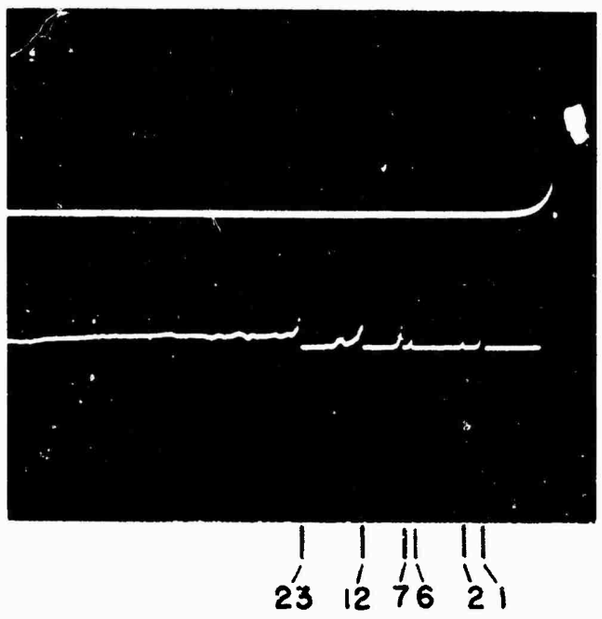

6b

Figure II-6 - Ion spectrum from (100) surface of single crystal nickel. a) before purging spectrometer with hydrogen. Lower trace is spectrum displayed at 2μs/cm. Upper trace is an expanded portion of the lower trace; b) after hydrogen purge. Lower trace is spectrum displayed at 2μs/cm. Upper trace is irrelevant. Time increases to the left in both cases.

as a very small peak; that led us to believe at first that hydrogen had no effect on the ion emission. However, after purging to 10^{-4} Torr, hydrogen became a very copious component of the spectra. Another important difference in the two spectra is that the absolute magnitudes of the alkali peaks are smaller in b than in a, indicating that the hydrogen has actually displaced some of the alkalies from the surface. Nevertheless, while our experiments show that it is possible to alter the composition of the surface coverage on single crystal nickel by leaking hydrogen into the system, they fail to show a single species hydrogen coverage. The reason for this apparent contradiction between the results obtained with laser irradiation and those from electron beam desorption [6], as well as low energy electron diffraction[7], may be due to the fact that the single crystal surface is more readily damaged by the laser probe[3]. It is also possible that the surface should be held at an elevated temperature in the presence of hydrogen for a longer time than has been possible with laser heating. We plan to heat the target for several hours by passing a current through it in the presence of hydrogen and then make further measurements of ion emission.

The single crystal nickel experiments, while failing, to date, to provide us with a surface with single species coverage, have provided us with valuable support for some of the results obtained previously. In the nickel data we observed what we believe to be the first evidence of doubly ionized species in the ion spectrum. The presence of Na^{++} is difficult to establish because of its proximity in the spectrum of $(C^{12})^{+}$, but we feel that we have established its identity beyond doubt. Figure II-7 is composed of three spectra from two different targets: II-7a is a spectrum from a polycrystalline graphite target and it is identical to Figure II-1; it is reproduced here to establish the position of the $(C^{12})^{+}$ peak in the spectrum by the arguments given in Section II-A, Ion Emission from Carbon. Figure II-7b is a spectrum from single crystal nickel

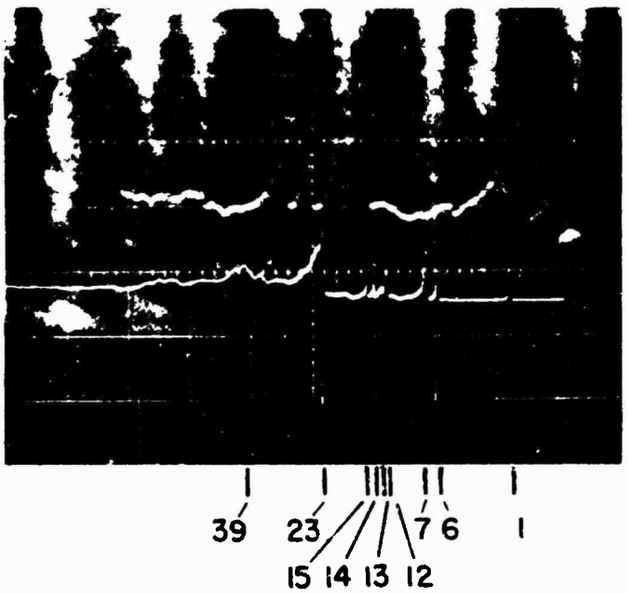

7a

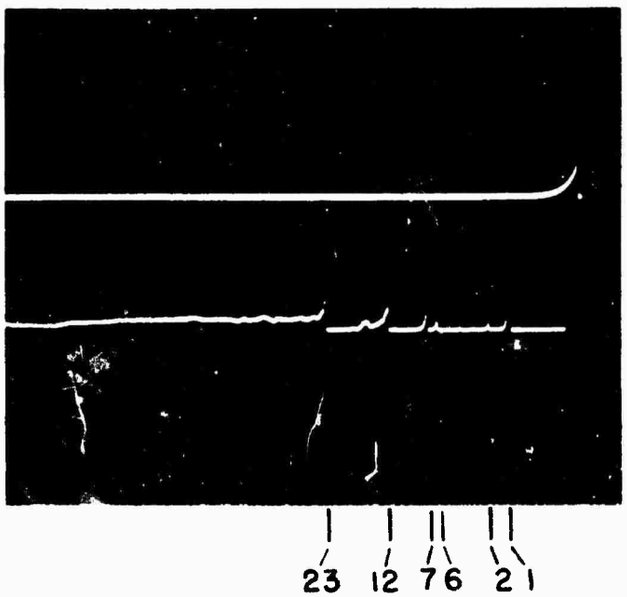

7b

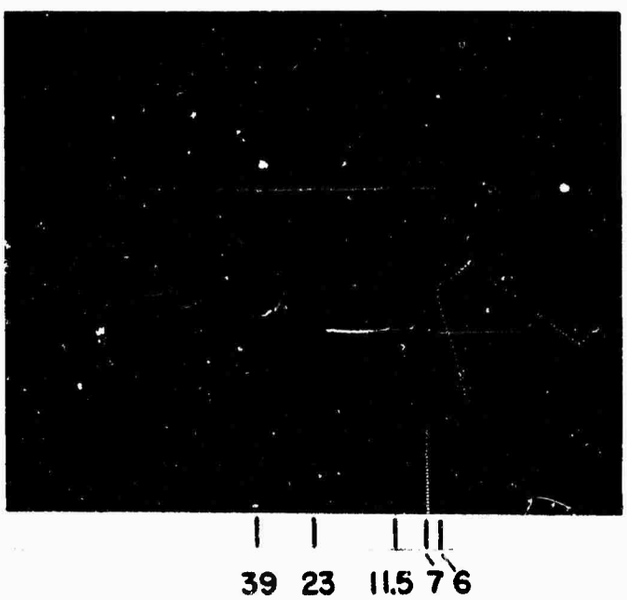

7c

Figure II-7 - Identification of Na^{++} in the ion spectrum. All spectra are displayed at 2 μs/cm with time increasing to the left. a) Ion spectrum from polycrystalline graphite used to identify position of $(C^{12})^{+}$ peak; b) Ion spectrum from nickel showing $(C^{12})^{+}$ peak at the same position as found in the spectrum from graphite; c) Ion spectrum from nickel showing Na^{++} peak at 11.5 amu/e.

showing the $(C^{12})^+$ peak at the same time as in II-7a; a very small peak can also be seen in this spectrum at 11.5 amu/esu. Figure II-7c is a spectrum from nickel showing a very large Na^+ peak at 23 amu/esu and a much smaller peak at 11.5 amu/esu. Now, if we assume that the Na^+ and Na^{++} are in thermal equilibrium we calculate, using the Saha equation and the measured ratio $Na^+/Na^{++} = 236$, a temperature of the initial plasma of $\sim$11 ev. The temperature obtained above is in very good agreement with the random component of energy obtained by using Allen's method for obtaining the velocity distribution of ions from the measured pulse shapes.[3] It does not account for the directed component of energy that is one order of magnitude higher. The above facts point out the need to examine the angular distribution of ion energies about the normal to the surface. Our plans for those measurements are described in a subsequent section.

The ion spectrum from nickel shown in Figure II-7b was obtained after the attempt to cover the surface with hydrogen, and it shows the first appearance of a peak at 2 amu/e observed in the TOF spectrometer. The peak corresponds to molecular hydrogen and its observation establishes a better cohesion with the data obtained in the quadrupole spectrometer where this species is very abundant.

The energies of the alkali ions in the nickel emission are comparable to, although slightly higher than, those found previously for tungsten and platinum surfaces. The energies of the nickel ions are comparable to those of the alkalies. Figure II-8 shows the ion spectra from the nickel surface before the hydrogen purge: a, b, and c are spectra taken with decelerating potentials of 0, 180, and 360 volts respectively. Examination of the figures indicates that Ni^+ ions with initial energies in excess of 180 ev are present in the emission, as well as alkalies with initial energies above 360 ev. The nickel ions are observed at a slightly shorter time than one would expect, but their identity is established by the same enhancement method used for the identification of $(C^{12})^+$ which is discussed in the previous section.

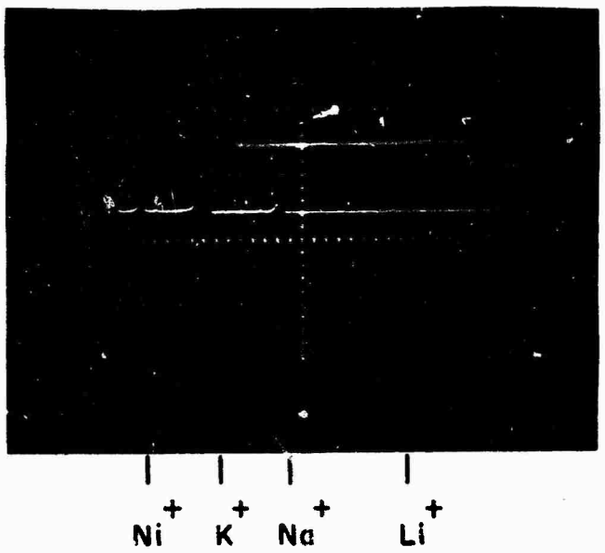

8a

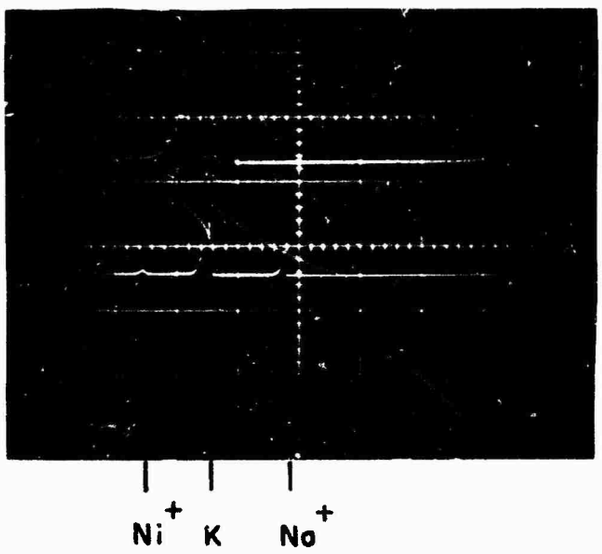

8b

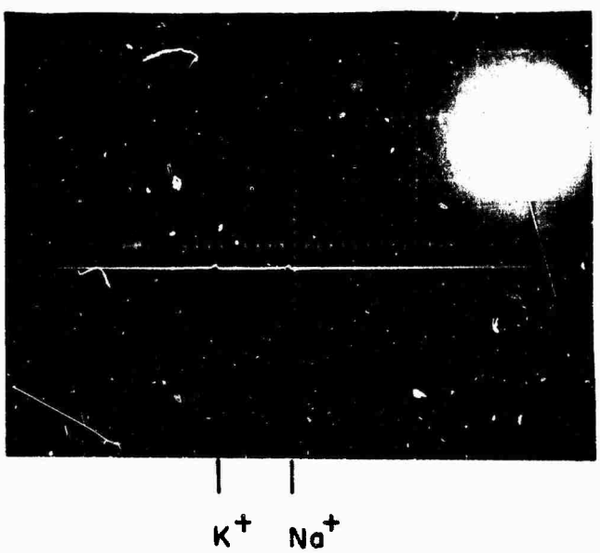

8c

Figure II-8 - Ion spectra from single crystal nickel. Lower trace is spectrum displayed at 2μs/cm with time increasing to the left. Upper trace is expanded portion of lower trace. a) no decelerating potential; b) 180 volts decelerating potential; c) 360 volts decelerating potential; the upper trace did not trigger in this picture.

C. S ARKING IN THE TOF SPECTROMETER

We have experienced considerable difficulty in trying to extend our time-of-flight measurements to higher optical flux densities. The reason for the difficulty is that when the flux density at the target reaches a value of about 70 megawatts/cm^2 a bright luminous front can be seen moving from the target to the accelerating grid; at the same time the signal from the electron multiplier detecting the ions becomes very erratic, at times dipping below the base line.

Attempts to restore a normal multiplier signal by putting a 10 μf capacitor across the power supply feeding the accelerating region only had the effect of causing the entire lower section of the spectrometer to glow. The problem with the multiplier signal was finally traced to a moving ground in the laboratory due to the large current drain in the target region. It was solved by using batteries in parallel with a .1μf capacitor to supply the accelerating region. However, once the noise was eliminated from the multiplier signal, it became apparent that the ion signal had also disappeared.

We believe we have now traced the loss of signal to losses in the electrical lead supplying the high voltage to the target. Figure II-9 is a photograph of the lower end of the TOF spectrometer[1] during irradiation of the target with a flux density of 70 megawatts/cm^2. A 10 μf capacitor was in parallel with the +2000 V dc supply connected between the target and the drift tube. One can easily see the plume emanating from the target and moving towards the drift tube. A very bright emission can also be seen from a section of the electrical lead that carries the high voltage from the feed-through at the bottom of the spectrometer to the target. The point of contact between the lead and the target is also very bright, indicating a high contact resistance.

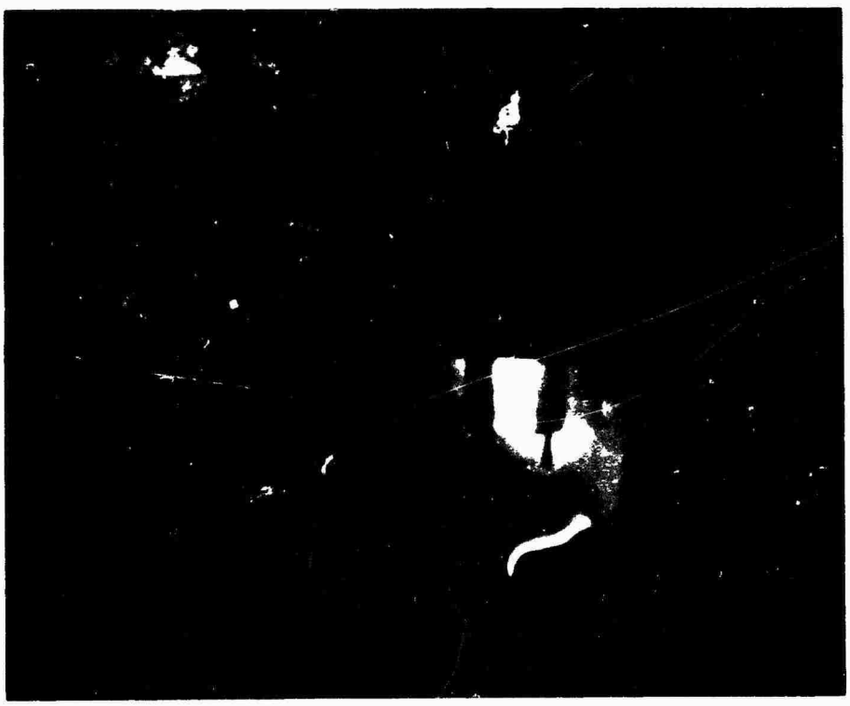

Figure II-9 - Photograph of lower section of TOF spectrometer during irradiation of target with flux density of 100 megawatts/cm^2. Luminous front can be seen emanating from target.

The peak current in the accelerating gap during sparking was measured by measuring the voltage drop across a 1 ohm resistor in series with the target. Peak currents of 100 amperes have been measured in pulses of full width of approximately 2 μs. Now, since the lead resistance inside the spectrometer is $\sim$1 ohm and the lead-to-target contact resistance is apparently higher, judging from the brightness of the glow, it becomes apparent that for high currents the target potential is only a small fraction of the nominal supply value. Hence, ions will not be accelerated efficiently into the drift tube.

During the next reporting period efforts will be made to correct this problem by providing a low resistance contact to the target. The accelerating grid will also have to be modified, because the large currents encountered destroy the type being used at present.

SECTION III

WORK ON QUADRUPOLE SPECTROMETER

This section describes work performed on the quadrupole mass spectrometer. In our earlier reports[1, 2, 3] we have discussed the neutral gas desorption observed in the normal operation of the spectrometer and the production of high energy neutral molecules, when the neutral gas pulse is eliminated. This earlier work was mainly based on tungsten targets.

We here describe data obtained from other target materials, nickel, titanium, and carbon. Some of the work, on nickel and titanium, has been partially reported earlier[3], but we describe it in more detail here. We also describe measurements on the effect of the laser power density on the amplitude and energy of the high energy neutral molecule pulses and we discuss the effect of spectrometer condition on the measurements of high energy neutral molecules.

The main features of the emission, both gas pulse and high energy neutral molecules, are similar from one material to the next. There are, however, definite and reproducible differences between materials. Since we have already reported the more important features in conjunction with our earlier description of the emission from tungsten, this report will take those features for granted and will place more emphasis on the finer differences in emission for different materials.

A. NICKEL TARGET

In a previous report[3] we described preliminary results obtained using a nickel target in the quadrupole mass spectrometer. As we mentioned in that report, we chose a nickel target because other work[6] indicated that the (100) face of single crystalline nickel could be treated in

such a way that it adsorbed only hydrogen and did not adsorb carbon monoxide. This result was based on electron beam probing of such a surface and analysis of the desorbed gas in a sector spectrometer,[6] where only desorbed hydrogen gas was observed. This is in contrast to observations made on most metallic targets in vacuum in which carbon monoxide is typically a dominant species.

In this report we shall review the preliminary results presented in the previous report[3] and then describe the additional work that has been perfcrmed using a single crystalline nickel target in the quadrupole spectrometer.

In contrast to the sector spectrometer work, we observe desorption of a number of species from the nickel target. We postulate that the difference between the two results lies in the much more violent nature of the laser bombardment as compared to the relatively more gentle nature of the electron beam probing. The surface is extensively damaged by the laser bombardment, as we mentioned in the previous report[3], as is shown by the fact that X-ray diffraction analysis indicates that the area struck by the laser beam has become polycrystalline. However, it does not appear that we can invoke disruption of the single crystalline form on one laser shot, followed by adsorption of various gases and then desorption by a later laser pulse. Even when we illuminate a fresh spot on the nickel surface for the first time, we find that gases other than hydrogen are emitted. This occurs even when the target had been heated previously with the system backfilled with hydrogen to a pressure about ten times the normal background. In fact, there appears to be no particular difference in the gases desorbed from a virgin spot as compared to a spot that has been struck before. The amount of gas desorbed per pulse from a given spot decreases slowly after the first pulse until it reaches a level about half the level produced in the first pulse, but it appears that several gas species

are desorbed in the first pulse that strikes a new spot. Thus, the most likely interpretation of the two diverse results is that the various gases, in particular CO, are in fact present on the surface, but are bound rather tightly, perhaps incorporated somewhat below the outermost layers, so that the electron beam does not dislodge them, while the more destructive effect of the laser beam can release them These results may be compared to the results obtained in ion emission from similar nickel targets (Section II), where multicomponent emission was also observed.

The largest component desorbed from nickel in the gas phase is in fact molecular hydrogen. The pulses at mass 28 are approximately half the size of the hydrogen pulses and those at mass 44 are about one fifteenth the size of the hydrogen pulses. Other masses commonly observed on other targets, such as water vapor and hydrocarbons, do not seem to be emitted in detectable amounts from the nickel. Thus, the amount of hydrogen observed in the gas phase is relatively enhanced using the nickel target as compared to other targets. In most targets the largest gas pulses occur at mass 28, and mass 2 pulses are somewhat smaller. Thus, there is evidence that the gas desorbed from our nickel targets is relatively richer in hydrogen, but hydrogen is by no means the only gas observed.

The high energy neutral molecule pulses emitted from the nickel target are somewhat different and more complicated than those produced when other target materials, e.g., tungsten, are used. A typical example is shown in the top photograph of Figure III-1. The first small peak is apparently hydrogen. It generally disappears, or is greatly reduced in size, when the target is heated, although there have been a few cases in which this peak was not affected by raising the temperature of the target. Figure III-1 shows the usual case. In the top photograph, taken with a cold target, the peak is present, and in the bottom photograph, taken with a heated target, this peak has disappeared. With the identification as hydrogen,

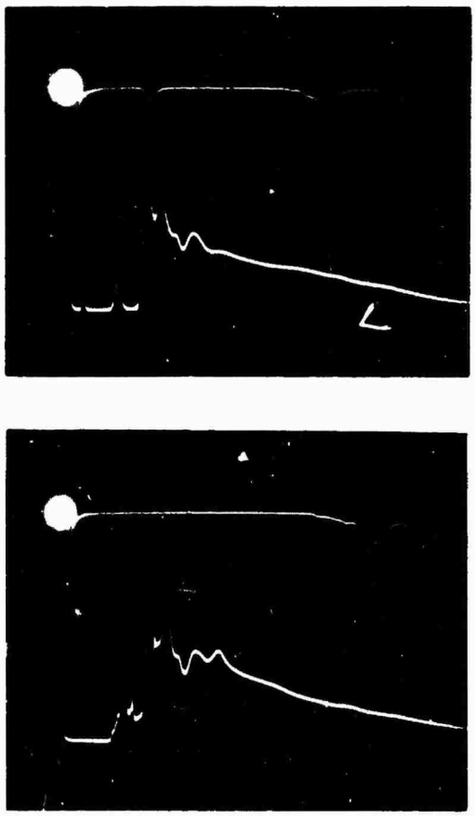

Figure III-1 - Neutral molecule pulses from nickel. Time increases toward right. Upper Traces: 0.5 volt/cm, 20 μs total sweep. Lower Traces: 0.2 volt/cm, 100 μs total sweep. Top photograph: target at room temperature. Bottom photograph: target heated.

the energy would be about 200 ev. The other peaks shown in Figure III-1 are not significantly affected by target temperature. The identifications of these later peaks are not certain, although the arrival times of the two largest peaks in Figure III-1 are consistent with CO and CO_2 if the first peak is in fact hydrogen. It appears somewhat odd that the largest pulse observed in the gas phase should be hydrogen, when it is realized that the hydrogen contribution to the high energy neutral molecule pulses is relatively small. This apparently argues that the acceleration mechanism operates differently on different species, or perhaps that the lighter gas diffuses away before the acceleration occurs.

Another puzzling feature noted on the high energy neutral pulses is that the hydrogen peak disappeared after several days of data taking. The peak corresponding to the first small peak in Figure III-1 gradually became smaller over a period of a few days and eventually was entirely absent, whether the target was hot or cold. Leaking in hydrogen gas to a pressure about ten times the normal background pressure (about 10^{-8} mm Hg) did not cause this peak to reappear. At the same time the hydrogen contribution to the neutral gas pulses remained at its former size.

B. CARBON TARGETS

A considerable amount of work has been done during this report period using carbon targets. Both amorphous carbon and pyrolytic graphite[4] were employed as target materials. In this work, the laser beam was focused so that the power per unit area reached higher values than have been used with previous target materials.

The results from the two types of carbon targets were very similar and no systematic difference in the emission from the two was noted.

The gas pulses from the carbon target were very similar to those observed earlier from other targets, such as tungsten. Gas pulses were observed at masses 2, 16, 18, 28, and 44. The largest pulses were at mass 28, corresponding to carbon monoxide. The hydrogen pulses at mass 2 were smaller by a factor of about two or three. This points out the relative enhancement of hydrogen desorption using the nickel target, as was described above. The carbon dioxide, mass 44, pulses were somewhat smaller than the hydrogen, and the mass 16 and 18 pulses were about an order of magnitude smaller yet. No detectable emission was noted at mass 12.

Some data were obtained on the amount of CO desorbed from the carbon target as a function of laser power density. The laser power was varied by inserting dielectric mirrors in the beam. This process apparently introduces additional scatter in the results, but is procedurally easier than varying the power output of the laser over a specified range. The general features were similar to results obtained earlier with tungsten and presented in Figure III-4 of an earlier report[2]. There is a threshold value for a measurable gas desorption pulse at 10 to 15 megawatts/cm^2, followed by a roughly linear increase in gas pulse size with increasing laser power density. Using the calibration of peak pulse height described in the earlier report[2] to obtain the absolute numbers of CO molecules desorbed per pulse, we find that at a given laser power the amount of CO desorbed from the carbon target is about 4 to 8 times as large as the amount desorbed from tungsten.

Some high energy neutral molecule pulses from the carbon targets are shown in Figure III-2. In this figure the upper photograph is data taken using an amorphous carbon target, and the lower photograph is data taken using a pyrolytic graphite target. We see that there is no systematic difference between the results from the two different types of carbon target.

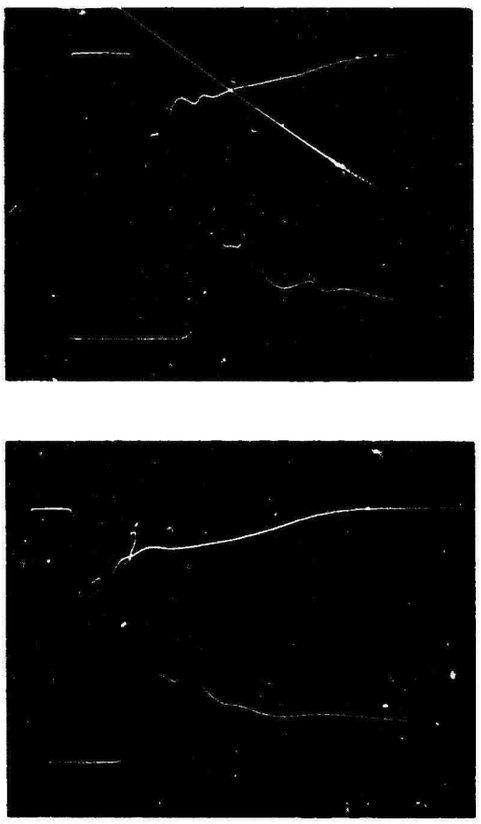

Figure III-2 - Neutral molecule pulses from amorphous carbon (top photograph) and from pyrolytic graphite (bottom photograph). Time increases toward right. Upper traces: 100 μs total sweep. Lower traces: 50 μs total sweep. All traces: 0.2 volt/cm.

This bears out the earlier statement that the emission from pyrolytic graphite and from amorphous carbon is very similar. The main feature of the pulses in Figure III-2 is the presence of two large spikes. These spikes are approximately equal in amplitude and occur at about 15 and 20 microseconds after the pulse of laser radiation. Pulses of this type are very consistent and reproducible features of the high energy neutral molecule emission from carbon. The relative times of arrival for a number of pairs of spikes are shown in Table III-1. We note that there is a considerable amount of scatter in this data.

Also listed in Table III-1 are accelerating voltages applied to the target. There appears to be no systematic difference in arrival time of the pulses with the applied accelerating voltage. The pulse to pulse variation in arrival times is large, but the applied voltage appears to make no difference. There are comparable variations between arrival times for zero applied voltage and between arrival times for zero and non-zero voltages. There does appear to be a trend toward earlier arrival times for later data points, but this is independent of applied voltage. Also shown are the ratio of the masses corresponding to these two spikes on the assumption that they correspond to the same energy. These ratios also have a considerable amount of scatter in them, but are consistent with the identities being CO and CO_2. The amount of scatter, however, precludes a certain identification. If these two spikes do in fact correspond to CO and CO_2, then the energies deduced from the time of flight would be approximately 225 ev. In none of the data taken with carbon targets is there any evidence of an early arriving pulse which could be identified as hydrogen. The presence of a hydrogen peak is a common feature of the emission from tungsten, titanium, and nickel; but it appears to be absent from the carbon targets. We will return later to the subject of the scatter in the arrival times and ratios shown in Table III-1.

TABLE III-1

TIMES OF ARRIVAL FOR THE TWO SPIKES IN THE HIGH ENERGY NEUTRAL MOLECULE PULSES FROM CARBON FOR A SERIES OF LASER SHOTS.

Arrival Time 1st Pulse (Microseconds)	Arrival Time 2nd Pulse (Microseconds)	Potential Between Target and Spectrometer (Volts)	Calculated Mass Ratio For the Two Spikes
15 25	18.75	0	1.51
14.50	17.50	0	1.46
15.50	20.50	-360	1.75
15.75	18.75	-360	1.42
14.00	19.00	0	1.84
14.00	20.20	-540	2.10
12.50	17.50	0	1.96
13.00	18.25	+360	1.97
14.50	19.00	0	1.72
12.75	17 00	+540	1.77
11.75	16.50	+540	1.97
11.25	14.00	0	1.55

We have devoted a considerable amount of work to investigating the variation in the high energy neutral molecule pulses emitted from carbon as a function of the laser power density. Figure III-3 shows the effect of the laser power density on the neutral molecule pulses in a qualitative fashion. The top photograph was taken at 84 megawatts/cm^2. Here we see the typical two spike pattern arriving fairly early. The middle photograph was taken at 50 megawatts/cm^2. Under these conditions the two spikes are still visible, but they have moved to later times and become smaller in amplitude. We note also that the second pulse arrives relatively later compared to the first pulse. The bottom photograph shows the behavior at still lower power, 30 megawatts/cm^2. Under these conditions the second pulse has entirely disappeared and the first pulse arrives quite a bit later than under conditions of higher laser power. These data are shown in a more quantitative fashion in Figures III-4, III-5, and III-6.

Figure III-4 shows the arrival time for the first spike in the neutral molecule pulses from a carbon target as a function of laser power density. This variation has been followed over a broad range of laser power by means of inserting various dielectric reflectors in the beam between the laser and the target. There is some scatter to the data but the systematic variation shows up in a very marked fashion with the arrival time decreasing with increased laser power. Figure III-5 shows the arrival time for the second spike in the neutral molecule pulses from a carbon target as a function of the laser power density. Comparing these two figures on the arrival times of the two different spikes, we see that the slopes of the two curves are about the same. Also over a considerable range these curves may be approximated by a linear function. If we write t_1 for the arrival time of the first pulse, and t_2 for the arrival time of the second pulse, then $t_1 = c_1 - \alpha p$ and $t_2 = c_2 - \alpha p$ where the c's are constants, α is the slope of the curve, and p is the laser power. Thus the ratio R of the masses as calculated for a particular laser shot of power density p is given by:

$$R = \left(\frac{C_1 - \alpha p}{C_2 - \alpha p} \right)^2 .$$

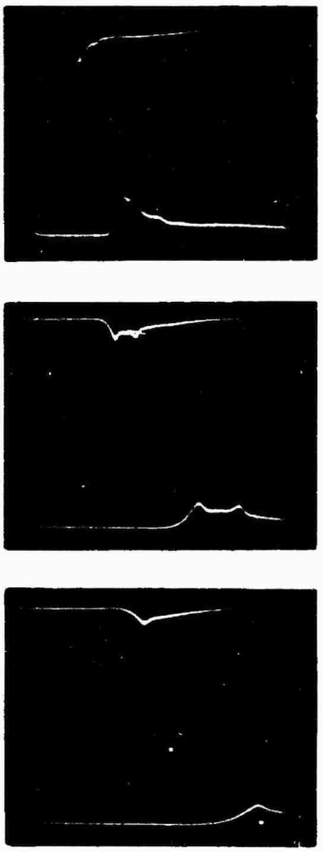

Figure III-3 - Effect of laser power on neutral molecule pulses from carbon.
Top photograph: 84 megawatts/cm^2.
Middle photograph: 50 megawatts/cm^2.
Bottom photograph: 30 megawatts/cm^2.
Time increases toward right. Upper traces: 100 μs total sweep
Lower traces: 50 μs total sweep. All traces: 0.5 volt/cm.

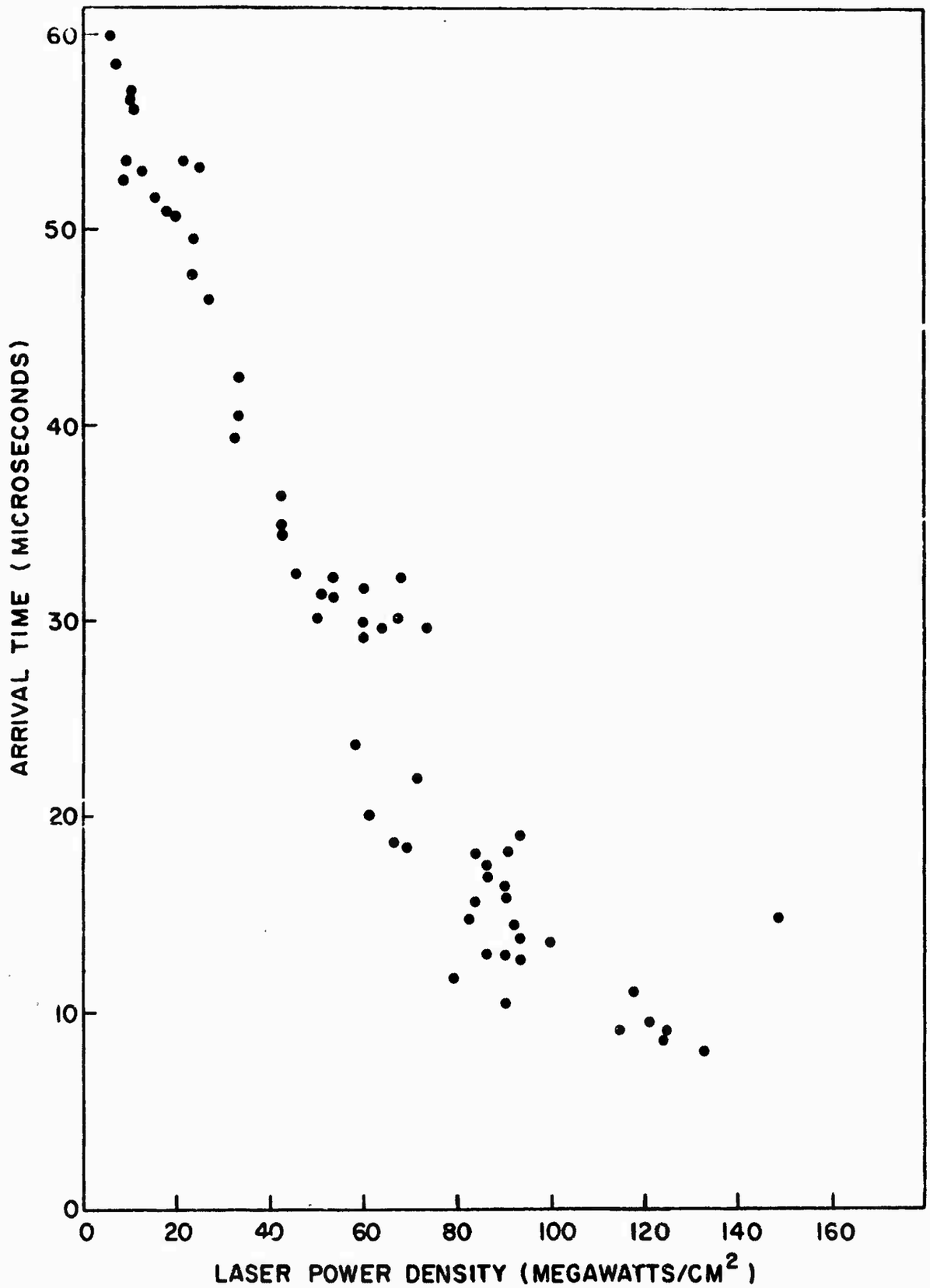

Figure III-4 - Arrival time of first neutral molecule pulse from carbon target as a function of laser power density.

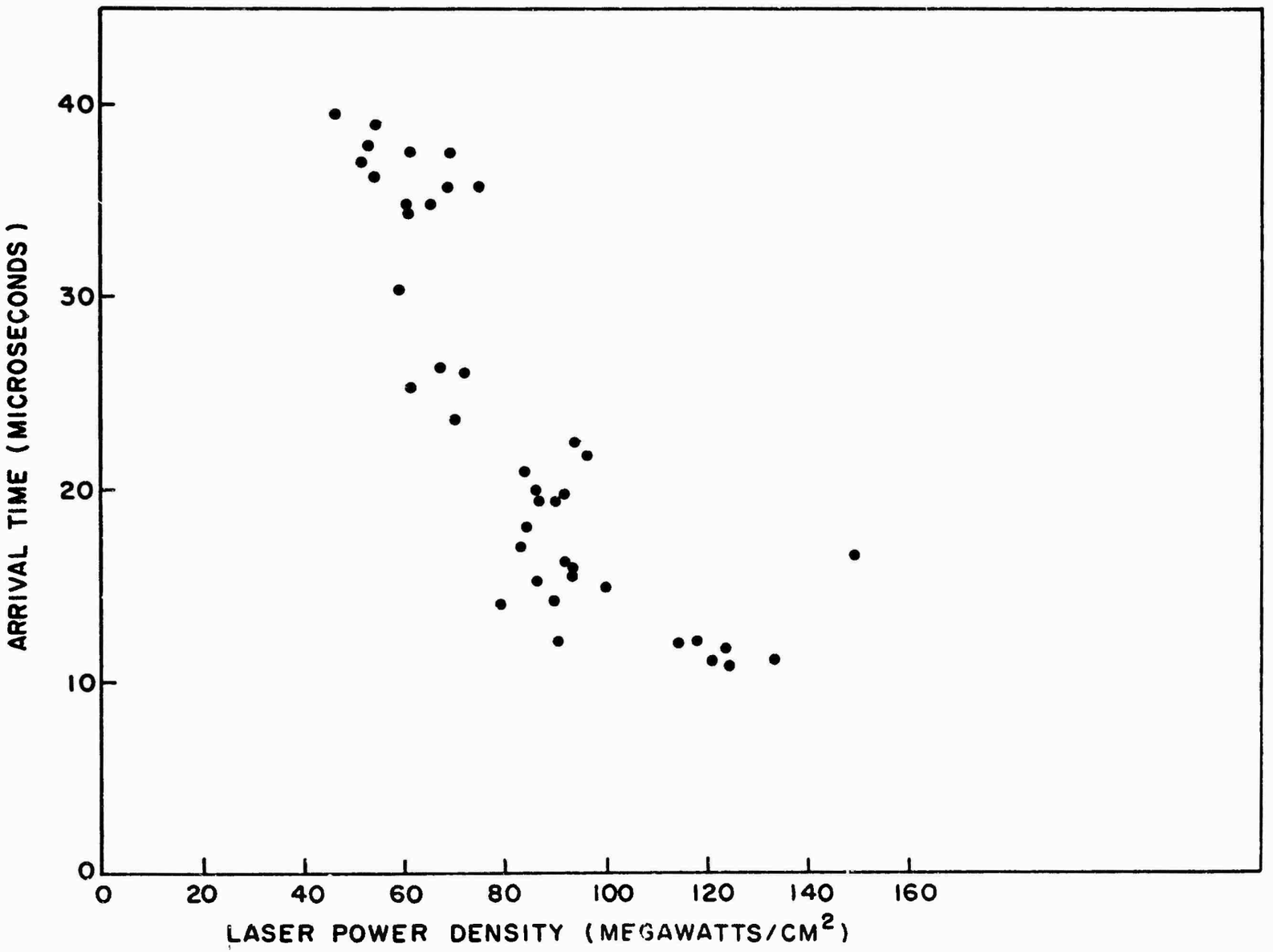

Figure III-5 - Arrival time of second neutral molecule pulse from carbon target as a function of laser power density.

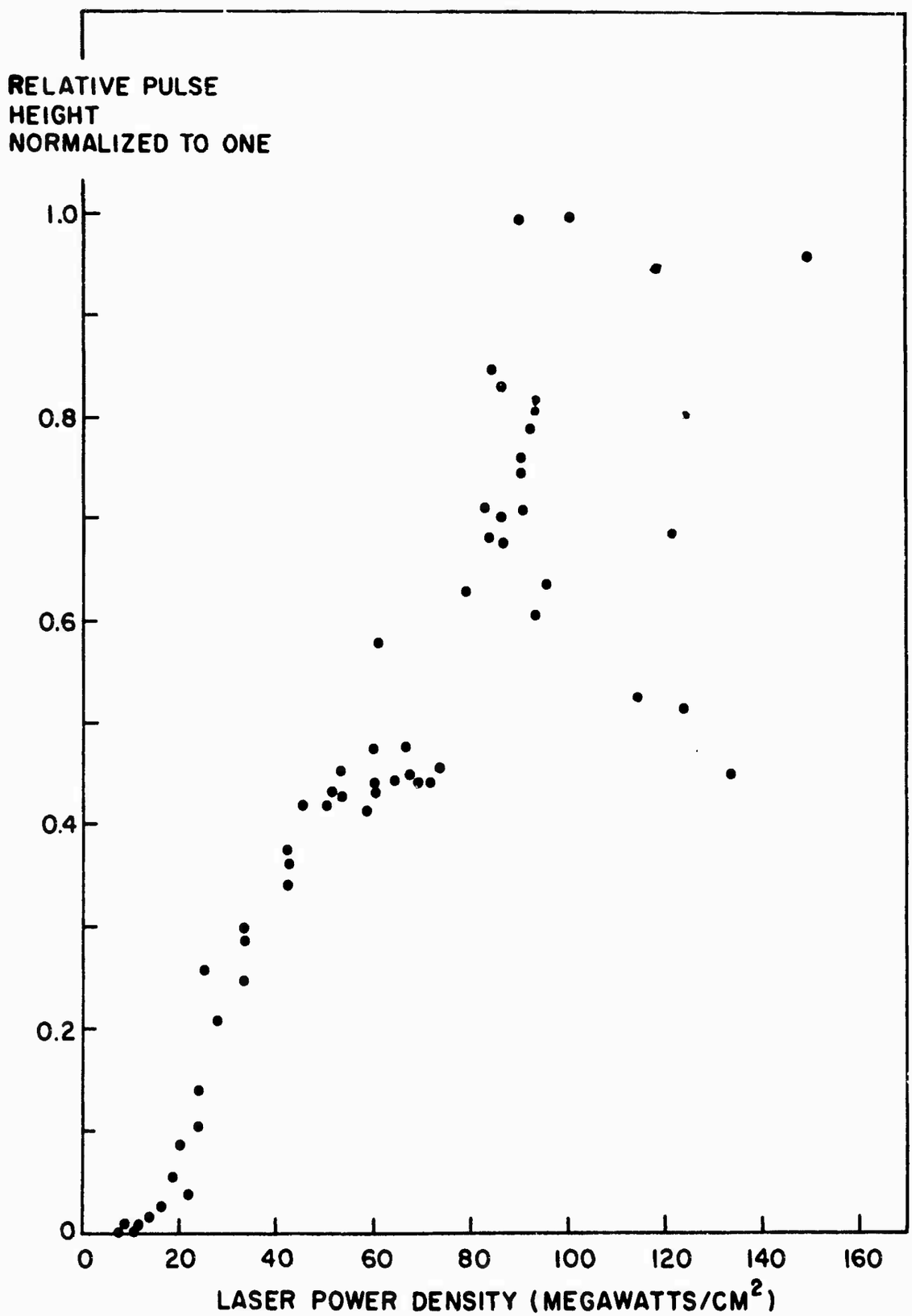

Figure III-6 - Relative height of first neutral molecule pulse from carbon target as a function of laser power density.

Therefore, the ratio R determined from a measurement of the arrival times from a particular photograph, will vary with the laser power. It will be different for different values of laser power. We regard this as a probable explanation for part of the scatter shown in Table III-1. The laser power varies somewhat from shot to shot in a random manner. This leads to the scatter of arrival times and the scatter of measured ratios R shown in that table.

From Figure III-4 we see that the energy of the particles constituting the first pulse can vary over a wide range. The energies at laser power densities exceeding 100 megawatts/cm^2 are over 400 ev per particle, if we assume that this pulse corresponds to CO, whereas at 20 megawatts/cm^2 the energy per particle would be only about 30 ev.

Figure III-6 shows the variation in the pulse height of the first spike in the high energy neutral molecule pulse from a carbon target as a function of the laser power density. There is a threshold around 10 megawatts/cm^2 below which we can detect no emission. Above 10 megawatts/cm^2 the pulse height rises fairly linearly up to about 60 megawatts/cm^2. At these higher power densities there is considerable scatter in the data and it is difficult to tell the form of the curve. Below 60 megawatts/cm^2 there is relatively little scatter and the points form a fairly smooth curve.

C. EFFECT OF SPECTROMETER CONDITION ON NEUTRAL MOLECULE PULSES

In the first work on high energy neutral molecule pulses, reported earlier[3], we observed that application of an accelerating voltage between the target and the entrance to the spectrometer apparently did not affect the high energy molecule pulses. Some later work with a titanium target indicated a contrary result; it indicated that application of a voltage between the target and the

entrance to the spectrometer did change the arrival times of the pulses, although the pulses did not disappear. This effect appeared at a relatively low applied voltage. In Figure III-7 we see some of these results. The top photograph shows pulses with the target grounded. The bottom photograph shows data under similar conditions with the target 4.5 volts positive with respect to the entrance of the spectrometer. The pulses arrive earlier in the lower photograph. This effect was quite reproducible. At relatively low voltages the change in arrival time was approximately linear with the applied voltage, but it saturated at around 100 volts, so that at higher voltages the arrival time was approximately constant. Application of a negative voltage between the target and the entrance to the spectrometer resulted in an increase in the arrival times of the pulses. It is rather surprising that the application of such a small voltage could cause this large an effect.

Since the pulses could not be eliminated even by application of very large decelerating voltages for ions, we concluded that the particles actually coming through the spectrometer must have been neutral. This led to the hypothesis that these particles spent part of their life as ions. Then the application of an accelerating voltage could change their energies. Later they would undergo charge exchange collisions and pass through the spectrometer as neutral particles. However, the amount of change with relatively small applied voltages was surprisingly large.

Before considering these results in more detail, we should review the operation of the spectrometer. Ordinarily the spectrometer is used in a condition in which neutral molecules diffusing from the target region enter an ionization chamber where a small fraction of them are ionized by an electron beam. These ions are then accelerated into the region where voltages applied to four rods cause a resonance condition for ions of a particular mass. Only ions of this particular mass can pass through the resonance region and reach the detector. A voltage on the detector assures that only positive particles will be detected. In

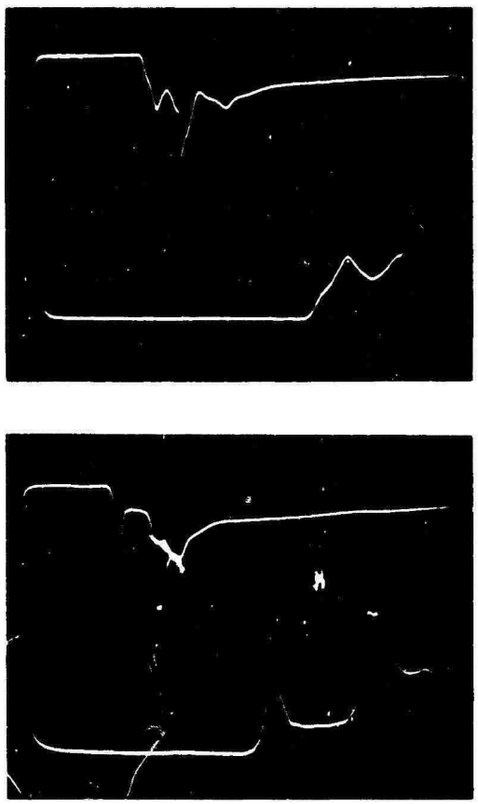

Figure III-7 - Effect of applied voltage on emission from titanium target.
Top photograph: target grounded
Bottom photograph: target at +4.5 volts.
Time increases toward right.
Upper traces: 50 μs total sweep. Lower traces: 20 μs total sweep.
All traces: 0.5 volt/cm.

measurements on the neutral gas emission the spectrometer is used in this condition. In measurements on high energy neutral particle emission, the ionization chamber was turned off so that the neutral gas emitted from the target region with low energy produced no signal. (A low energy neutral molecule reaching the cathode of the multiplier does not produce a secondary electron.) We noted that a small rapidly arriving signal persisted. The signal remained even when the spectrometer was tuned opaque for all charged particles. By applying electric and magnetic fields we assured ourselves that this signal actually arose from passage of high energy neutral particles from the region of the target through the spectrometer to the detector.

The spectrometer can also be used in a different condition. In this condition the spectrometer is turned entirely off. All voltages are removed from the four rods that make up the quadrupole. The ionization chamber is off. In this condition the spectrometer is in effect merely a tunnel through which particles can pass from the target to the detector. Some early work using a tungsten target seemed to indicate that it made relatively little difference in the neutral molecule pulses whether the spectrometer was used in this off condition, or whether it was used in the opaque condition in which the voltages are applied to the quadrupole so as to eliminate passage of all positive ions through the system. In the off condition, of course, the normal neutral gas pulse would not be present because none of the gas molecules would be ionized in the ionization chamber. This preliminary conclusion, that the condition of the spectrometer did not affect the high energy neutral molecule pulses, was erroneous as we shall see shortly. This interpretation led to the anomalous results with the titanium target as described above. Further measurements described later clarify the effect of the spectrometer condition.

Still another variation in the condition of the spectrometer arises from the presence of various grids in the ionization chamber. These grids may either be grounded or may be left floating. In the measurements conducted on the

titanium target, and shown in Figure III-7, in which it appeared that application of a voltage between the target and the spectrometer resulted in change of the arrival time of the pulses, the spectrometer had been used in the off condition with the grids and the ionization chamber ungrounded. Because of the unexpected nature of the results shown in Figure III 7 and because earlier work with the tungsten target had indicated that application of a voltage caused no difference in the arrival time of these pulses, we returned to a tungsten target. Some results taken with this target are shown in Figure III-8. In this figure we see the emission from a tungsten target. In the upper photograph the spectrometer is in the opaque condition with all grids in the ionization chamber grounded. In the lower photograph the spectrometer is in the off condition, that is, all voltages are removed from the quadrupole and the system acts merely as a tunnel through which particles can pass. The grids in the ionization chamber were floating. The data in the upper photograph is very similar to the results obtained earlier[3] from the tungsten target. The lower photograph shows a much larger emission. This indicates clearly that the condition of the spectrometer, whether it is off or opaque and whether the grids are grounded or floating, does indeed make a considerable difference in the character of the emission observed at the detector when the ionization chamber is off. This difference had not been recognized at the time the data in Figure III-7 were taken.

Figure III-9 shows results taken with a voltage applied to the tungsten target. In the top photograph the target is grounded, in the middle photograph the target is at 540 volts positive relative to the spectrometer; and in the bottom photograph the target is 360 volts negative relative to the spectrometer. These results were all taken with the spectrometer opaque, and with all the grids grounded, and they reproduce faithfully the results obtained earlier[3] with the tungsten target. Figure III-9 shows that application of a voltage affects neither the arrival time nor the pulse height of the high energy neutral

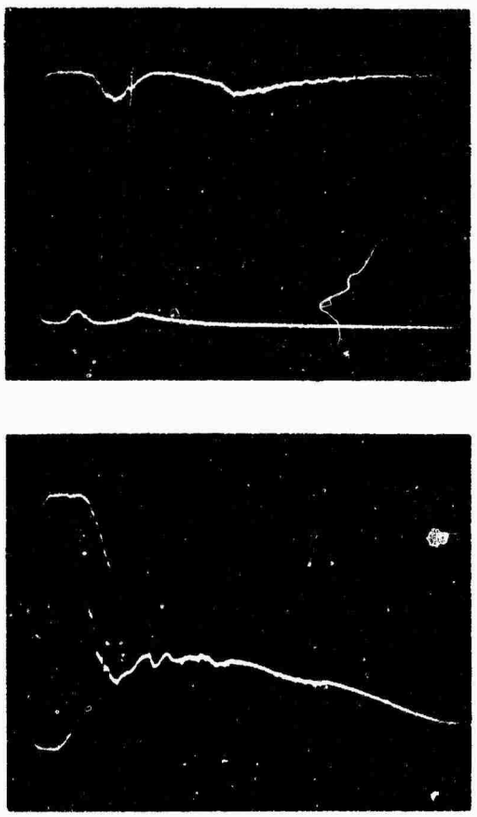

Figure III-8 - Emission from tungsten target. Upper Photograph: spectrometer opaque. Lower photograph: spectrometer off. Time increases toward right. Upper traces: .2 volt/cm and 50 μs total sweep. Lower traces: .5 volt/cm and 100 μs total sweep.

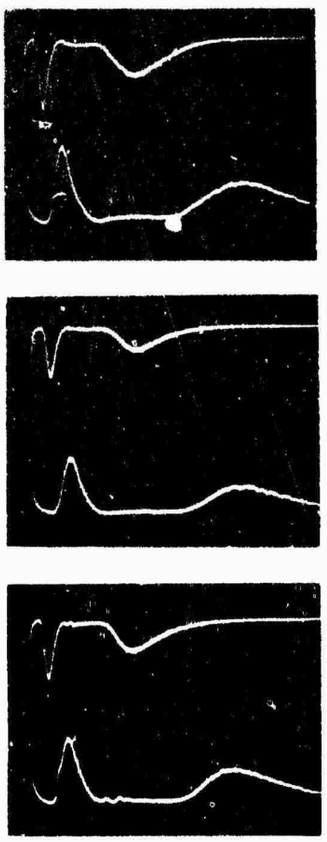

Figure III-9 - Neutral molecule pulses from tungsten, spectrometer opaque. Top photograph: target grounded; middle photograph: target +540 volts; bottom photograph: target -360 volts. Upper traces: 100 μs total sweep. Lower traces: 50 μs total sweep. All traces: 0.1 volt/cm.

molecule pulses. From the results of Figure III-8 and III-9 we conclude that the high energy neutral molecule emission is properly measured with the spectrometer in an opaque condition. With the spectrometer in the off condition spurious signals can be obtained. The most probable cause of these signals is charged particles hitting the grids in the ionization chamber and causing secondary emission which reaches the detector. Another possibility is that there may be ion emission, similar to what is observed in the time-of-flight spectrometer. These ions reach the detector when the spectrometer is in the off condition and contribute to the background shown in Figure III-8 in the bottom photograph. These results show clearly that the condition of the spectrometer in these measurements is important and that not taking proper account of the condition of the spectrometer can lead to spurious results.

Because of the possibility of additional undesired emission from the grids in the system, we made one further check on the identification of the particles in the high energy neutral molecule pulses. We inserted a grid after the quadrupole part of the system. To this grid we could apply another decelerating voltage for charged particles. Results of these measurements are shown in Figure III-10. These show the neutral molecule pulses from a grounded tungsten target. In the top photograph the additional grid is grounded. In the middle photograph the grid was at a positive potential of 360 volts, and in the bottom photograph at a negative potential of 540 volts. It is apparent that the voltage on this grid does not affect either the arrival times or the amplitudes of the high energy neutral molecule pulses. This indicates that these pulses do not originate within the spectrometer, but are in fact neutral particles that travel from the target to the detector. This result gives an added confirmation to our earlier conclusion on the nature of these pulses. This conclusion had been somewhat confused by the results using the spectrometer in an off condition and the various grids in the ionization chamber ungrounded but the work described here has clarified the cause of these spurious results and confirmed our earlier interpretation.

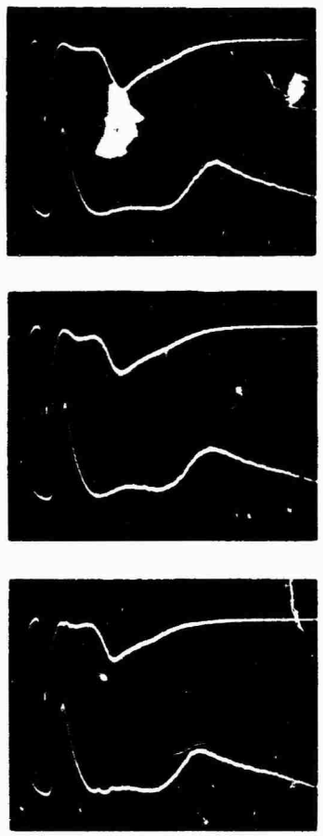

Figure III-10 - Neutral molecule pulses from grounded tungsten target. Top photograph: grid grounded. Middle photograph: grid + 360 volts. Bottom photograph: grid - 540 volts. Time increases toward right. Upper traces: 100 μs total sweep. Lower traces: 50 μs total sweep. All traces: 0.1 volt/cm.

From the results described above, it is apparent that the proper way to measure these pulses is with the spectrometer opaque and with the grids properly grounded. The results of Figure III-9 and III-10 taken together show clearly that the pulses we are interpreting as neutral molecule pulses spend no part of their life as ions, but must be neutral particles coming from the target to the detector. We should note at this point that the data taken with carbon, described in an earlier section, were obtained using the spectrometer in its opaque condition.

D. TITANIUM TARGET

Using the knowledge gained in these measurements, we returned to a titanium target. Figure III-11 shows the emission from titanium under various conditions. In the top photograph the spectrometer is opaque and the target grounded. In the middle photograph the spectrometer is opaque and the target is at a positive voltage of 360 volts. In the bottom photograph the spectrometer is off and the target grounded. The vertical scales in all three photographs are the same. We see that when the spectrometer is off the pulse is much larger, so large as to obscure all the structure in the top two photographs. This emission shown in the bottom photograph is apparently spurious. The results in the top two photographs show the neutral molecule emission from titanium. This structure is quite repeatable under various conditions. Comparing the top two photographs we see that application of a voltage makes no difference in the arrival time of the pulses. This turns out to be a quite general result. As with tungsten, we now obtain no variation in arrival time when either a positive or negative voltage is applied to the titanium target. The results shown in the top two photographs are the true high energy molecule emission from tungsten. This emission was apparently obscured in the first measurements on the titanium target. However, even these measurements taken with the spectrometer in the off condition

Figure III-11 - Emission from titanium. Top photograph: spectrometer opaque and target grounded. Middle photograph: spectrometer opaque and target at + 360 volts. Bottom photograph: spectrometer off and target grounded. Time increases toward right. Upper traces: 100 μs total sweep. Lower traces: 50 μs total sweep. All traces: 0.2 volt/cm.

indicated a small peak which disappeared when the target was heated and which we interpreted as hydrogen. Figure III-12 shows the effect of heating the target. The top photograph was taken with the target cold. The middle photograph is taken with the target warm, approximately 100°C. The bottom photograph was taken with the target hot, several hundred degrees Centigrade. These results were all obtained with the spectrometer opaque. The effect of heating the target is quite marked. The initial fast arriving pulse decreases in amplitude and eventually disappears. This is a reproducible result. When the target is cooled, the first pulse reappears. There is some evidence that the later emission develops additional structure upon heating the target, but this effect is not clear. The first pulse in the high energy neutral molecule emission of titanium, which is the largest pulse in the top two photographs in Figure III-11 and in the top photograph of Figure III-12, can apparently be identified as hydrogen. With this identification the energies corresponding to this first pulse would range up to approximately 100 ev. This hydrogen pulse also showed up with the spectrometer off. It was a small pulse near the beginning of the emission which disappeared upon heating the target. However, with the spectrometer off, the subsequent emission was so much larger that this pulse appeared to be a relatively small portion of the total emission. With the spectrometer opaque the hydrogen pulse now becomes the dominant feature of the emission. There is a smaller pulse after the hydrogen pulse in Figures III-11 and III-12. It is difficult to identify this material because these pulses are broad and not very clear cut.

We have also investigated the variation of these pulses with laser power. The relative height of the first pulse, the hydrogen pulse, is shown in Figure III-13. Again we see a threshold near 10 megawatts/cm^2 and a roughly linear increase in amplitude with power. In Figure III-14 we see the relative height of the second broad pulse emitted from titanium. This pulse does not quite go to zero in the range 10-15 megawatts/cm^2.

Figure III-12 - Neutral molecule pulses from titanium with spectrometer opaque and target grounded. Time increases toward right. Upper traces: 100 μs total sweep. Lower traces: 50 μs total sweep. Top photograph: target cold, upper trace 0.5 volt/cm, lower trace 0.2 volt/cm. Middle photograph: target warm (~100°C), both traces 0.2 volt/cm. Bottom photograph: target hot (several hundred degrees C), upper trace 0.5 volt/cm, lower trace 0.2 volt/cm.

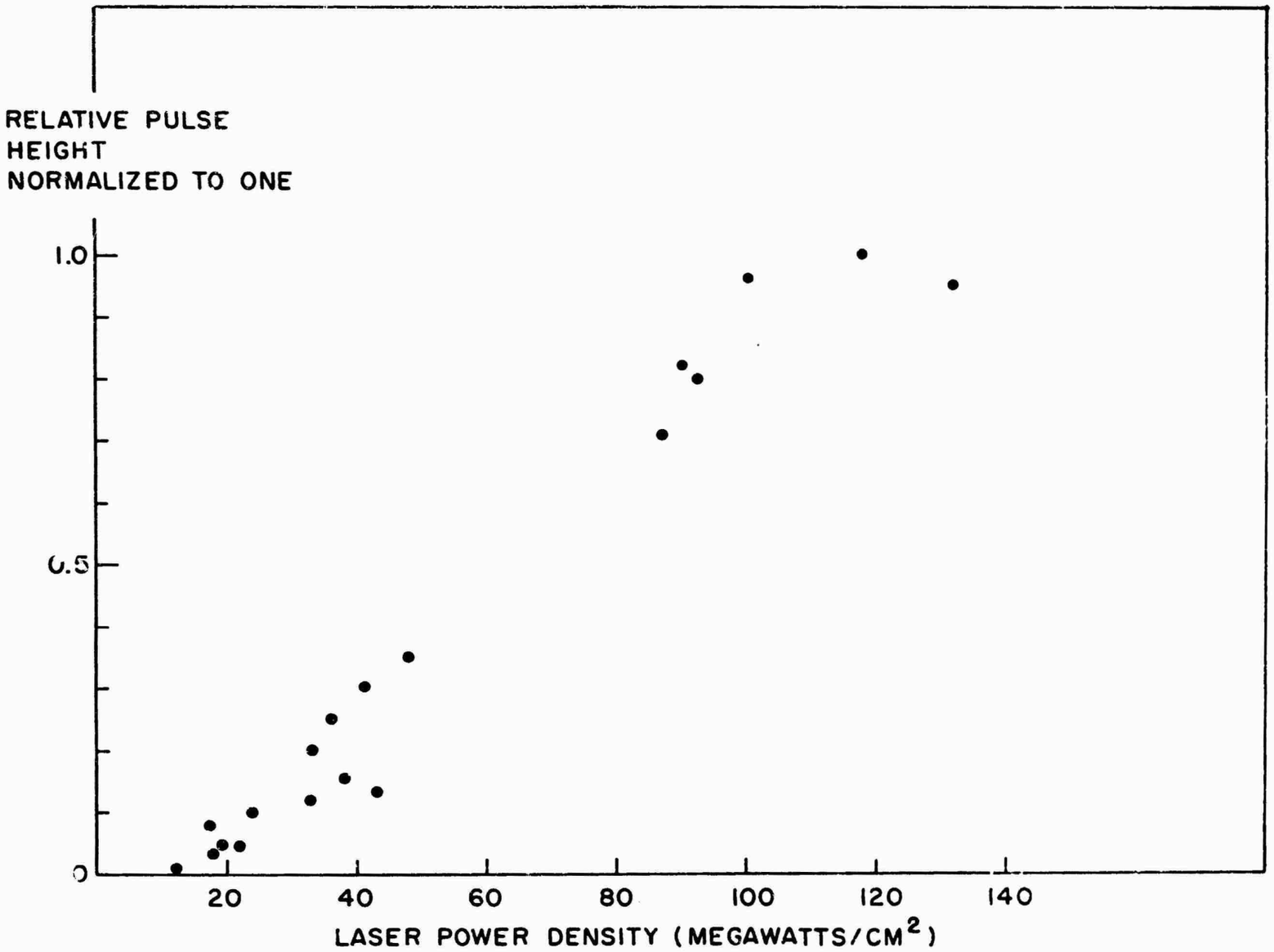

Figure III-13 - Relative height of first neutral molecule pulse from titanium target as a function of laser power

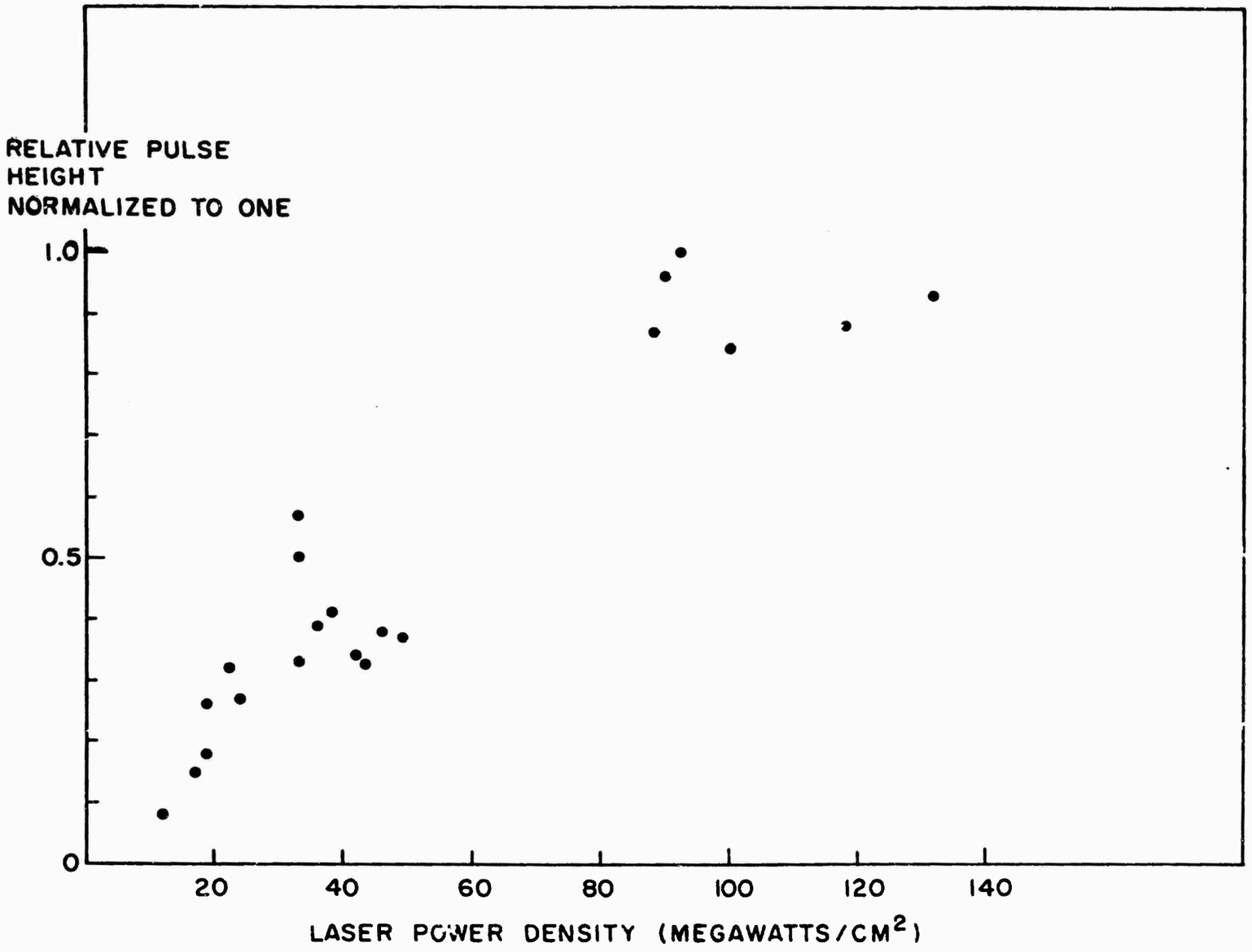

Figure III-14 - Relative height of second neutral molecule pulse from titanium target as a function of laser power.

Therefore, while at higher laser powers the pulses appear as in the top photograph of Figure III-12, at relatively low laser powers the first pulse disappears while the second pulse remains.

The variation of the arrival time of the first (hydrogen) pulse from titanium is shown in Figure III-15. Again, although the data has considerable scatter, there is a generally decreasing trend as power increases. The variation indicates that the hydrogen molecule energies increase from the 60-70 ev range at lower laser powers to the 90-100 ev range near 100 megawatts/cm^2.

E. CONCLUSION

To conclude this section on the quadrupole spectrometer, we review some of the results presented above. The work described here supports the conclusions described in an earlier report[3], in regard to the identities of the pulses observed when the ionization chamber is turned off and the neutral gas pulse disappears. However, the exact condition of the spectrometer is important, in that spurious pulses can occur and mask the neutral molecule pulses. In particular, the spectrometer should be turned opaque to all charged particles, and the grids in the ionization chamber should be grounded.

This work has been particularly concerned with the details of the high energy neutral molecule emission and its variations between different target materials and the dependence on laser power. The main components appear to be H_2, CO, and CO_2, a result which is compatible with the gas pulse analysis. However, considerable scatter in the data precludes certain identification. Apparently, much of the scatter is due to variations in laser power from shot to shot. The different pulses vary in different manners with the laser power, as was described in conjunction with Figures III-4 and III-5, so that the ratios of masses obtained on different shots will vary if the laser power varies.

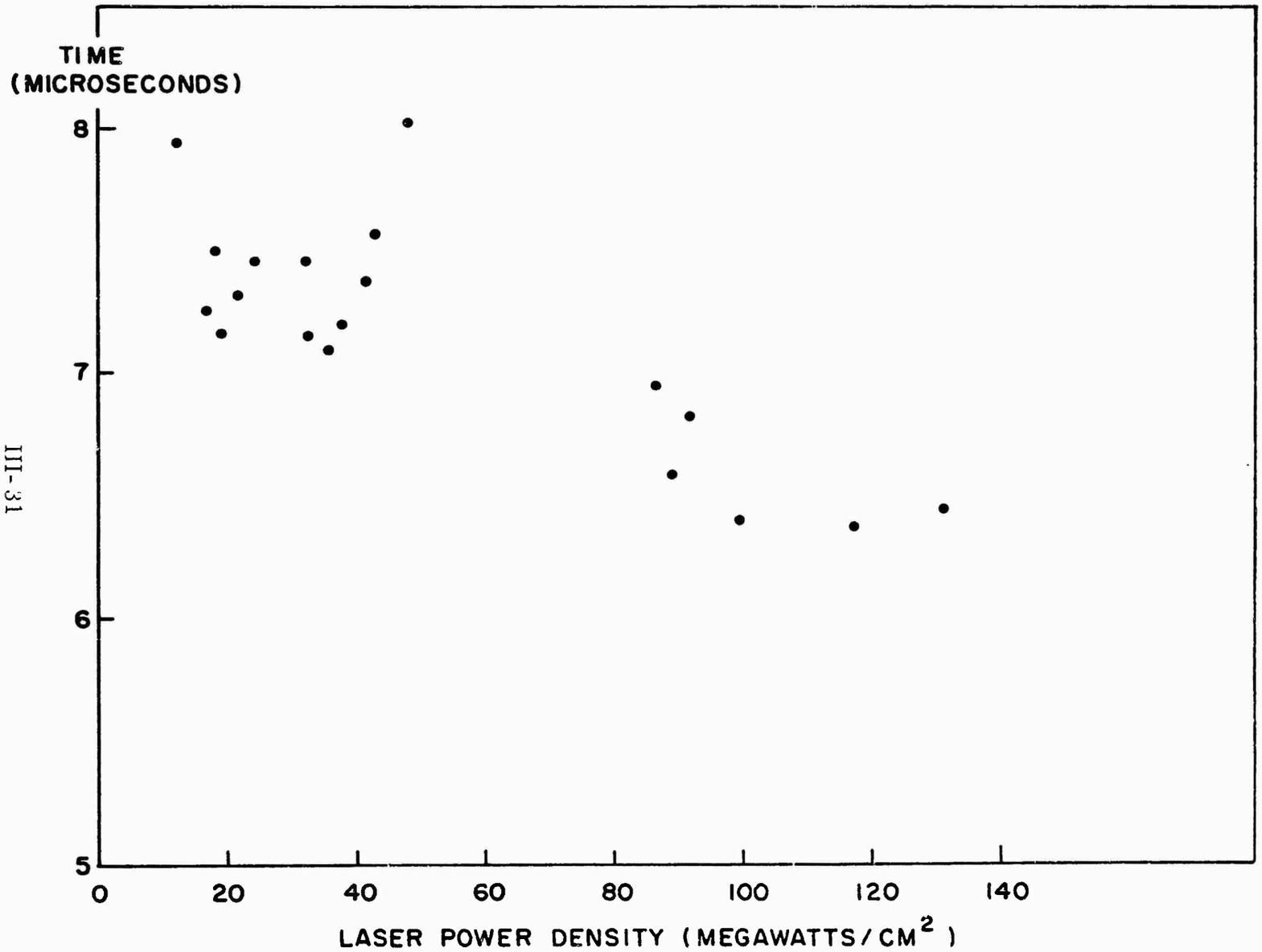

Figure III-15 - Arrival time of first neutral molecule pulse from titanium target as a function of laser power.

The quadrupole spectrometer was not designed for measurements of this type and is limited in its capabilities for energy measurements. Indeed, as we discussed earlier[3], high energy neutral particles offer difficulties for any type of measurement. The basic features of the high energy neutral molecule emission are broadly similar from one target material to another, although there are definite and reproducible differences. It is not the purpose of this work to examine differences among many different types of material, but to perform more general types of measurement to elucidate the nature of the laser-surface interaction. Accordingly, we intend in the near future to phase out the use of the quadrupole spectrometer in favor of apparatus more specifically designed to study the emission actually found to occur, i.e., the apparatus described in the next section.

SECTION IV

NEW EQUIPMENT

Two new major pieces of equipment have been designed and are being constructed. They are a new high vacuum interaction chamber and a high power laser. The interaction chamber will be used to measure angular distribution of numbers and energies of charged particles of both signs emitted upon irradiation of surfaces; it will also be used in an experiment to test directly the inverse Bremsstrahlung acceleration mechanism. The laser will be used for all future experiments requiring peak powers of the order of 100 megawatts.

A. INTERACTION CHAMBER FOR ANGULAR DISTRIBUTION MEASUREMENTS

A new interaction chamber has been designed and is being constructed that will allow us to check some of the assumptions that have been made in our experiments up to date; it will also enable us to perform an experiment to test experimentally the inverse Bremsstrahlung mechanism for ion acceleration.

The chamber, shown in Figure IV-1, consists of a high vacuum cylindrical stainless steel chamber with five optical windows. A target surface is placed near the bottom of the chamber, centered on the cylinder axis. The target is also at the center of a hemispherical shell that has twelve detectors mounted on its outer surface. Eleven of the detectors are located at equal intervals along one meridian of the hemisphere, while the twelfth is along a meridan perpendicular to the first and at thirty degrees from the polar axis. The detector openings in the hemisphere are oriented in such a way with respect to the top cover of the vacuum chamber, that the target can be irradiated through any of the three optical windows on the cover. There are two more windows located opposite each other on the sides of the chamber, through

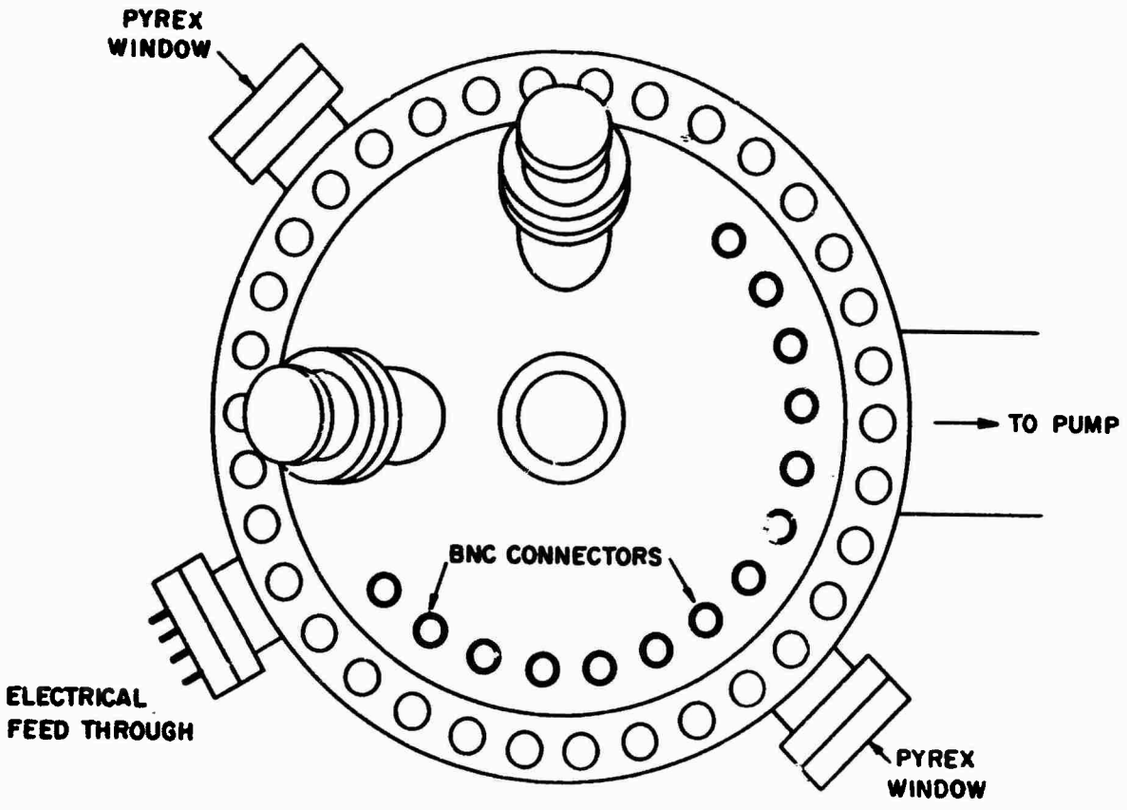

Figure IV-1a - Side view of interaction chamber

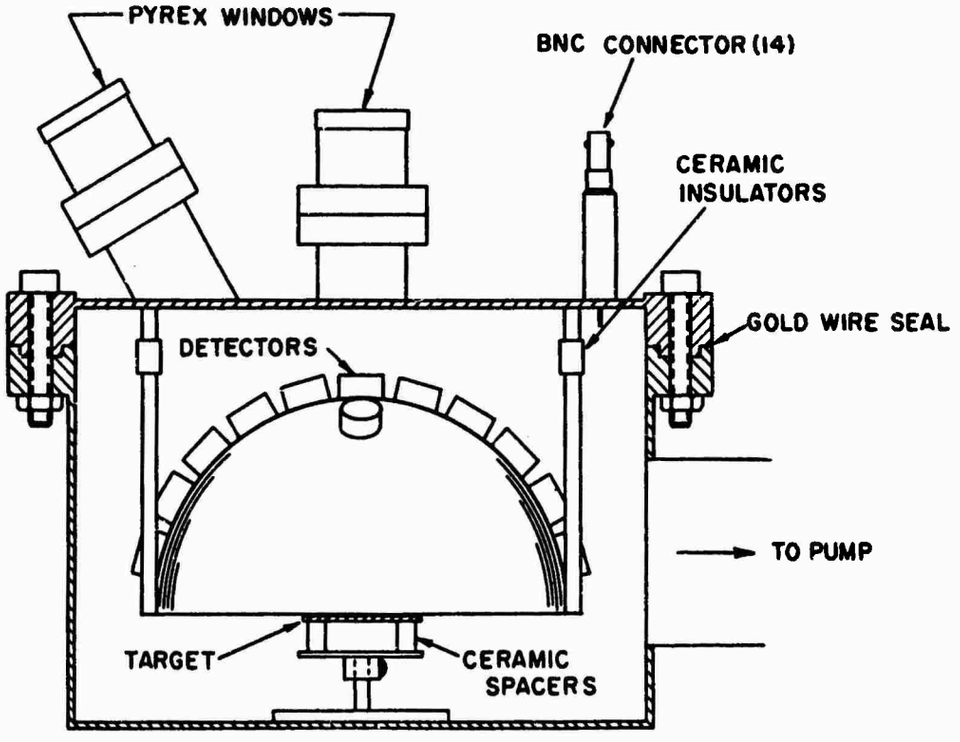

Figure IV-1b - Top view of interaction chamber

which a laser beam can be shot parallel to the target surface. The hemisphere and the target surface are electrically isolated from ground so that different potentials can be applied to them.

There are two types of detectors that will be used. The first will be a bipolar detector in which charges of both signs can be collected on two different electrodes without any energy discrimination, the second type will collect charges of one sign only, but will contain a decelerating grid that can be used to measure the energy of the particles collected. The output of each detector will be taken out of the vacuum chamber by means of a high vacuum coaxial connector.

The rather complicated array of detectors and ports described above will allow us to measure the angular distribution of particles emitted by the target upon irradiation with a beam normal to its surface, and at sixty degrees to the surface for two azimuthal directions at right angles to each other. Such experiments will allow us to test the validity of our assumption of near-isotropy of the particle emission, upon which the estimates of numbers of particles are based. Recent reports[8] indicate that there may be drastic departures from isotropy.

The same experiments used to measure the angular distribution of particles can be used to measure the angular distribution of particle energies. This can be accomplished either by applying decelerating potentials to the detector grids or by comparing the times of flight of particles to detectors located at different angular positions. This experiment will give us a check on our previous results, which indicated that most of the particle energy consists of a component directed away from the surface. It will also give some information about the acceleration mechanisms, since processes such as inverse Bremsstrahlung should not lead to acceleration in a preferred direction.

The chamber will also be used to measure properties of the electron emission upon irradiation. In our work to date we have assumed that charge separation occurs very near the target and that we can treat the particles as independent entities; this assumption has been justified on the grounds that the ions react to applied fields as independent particles. [3] On the other hand, experiments at high power densitites, using droplets that are evaporated by the laser beam, indicate that no charge separation occurs for many centimeters. [9] We will investigate whether or not charge separation occurs under our experimental conditions by measuring simultaneously the signals of both signs in the bipolar detectors. Also, we will attempt to determine the power density at which there is no longer charge separation. Such a measurement will enable us to determine the validity of our calculations of inverse Bremsstrahlung cross-sections, since the latter should increase sharply after that point due to the increased electron density. The energies of the emitted electrons will also be measured in this system.

An experiment will also be performed to test directly the hypothesis of inverse Bremsstrahlung heating. Essentially, the experiment will be a replica of our current experiments, where a 20-70 megawatts/cm^2 pulse is fired onto the surface, except that now a second laser will be shot parallel to the surface in order to intercept the blow-off material. The power density of the second beam will be at least one order of magnitude higher than that of the first, and its arrival time at the interaction region will be varied by using a variable length path. If inverse Bremsstrahlung is the mechanism involved in ion acceleration, we should observe a large increase in the energies of the ions produced.

B. HIGH POWER RUBY LASER

A Q-switched ruby laser is being built that will allow us to operate at considerably higher power densities than those used to this date. It will be used to examine the energies of both ions and neutrals that we have observed at the 20-70 megawatts/cm^2 level. It is also required for use in the experiments to test the inverse Bremsstrahlung hypothesis.

A schematic of the laser is shown in Figure IV-2. It consists of a 6 inch long ruby rod and a water cooled flashtube placed at the foci of a dielectric coated elliptical reflector. The ends of the ruby are cut at Brewster's angle. On one side the cavity is terminated by a Brewster angle roof prism; on the other end of the cavity is a 25% reflecting sapphire etalon. Inside the cavity will be two liquid Q-switch cells placed also at Brewster's angle. The use of two cells has been reported to produce more repeatable and shorter output pulses from this type of laser.[9]

We expect peak power outputs in excess of 100 megawatts from this laser, as compared to the 5 to 15 megawatts obtainable from our present lasers.

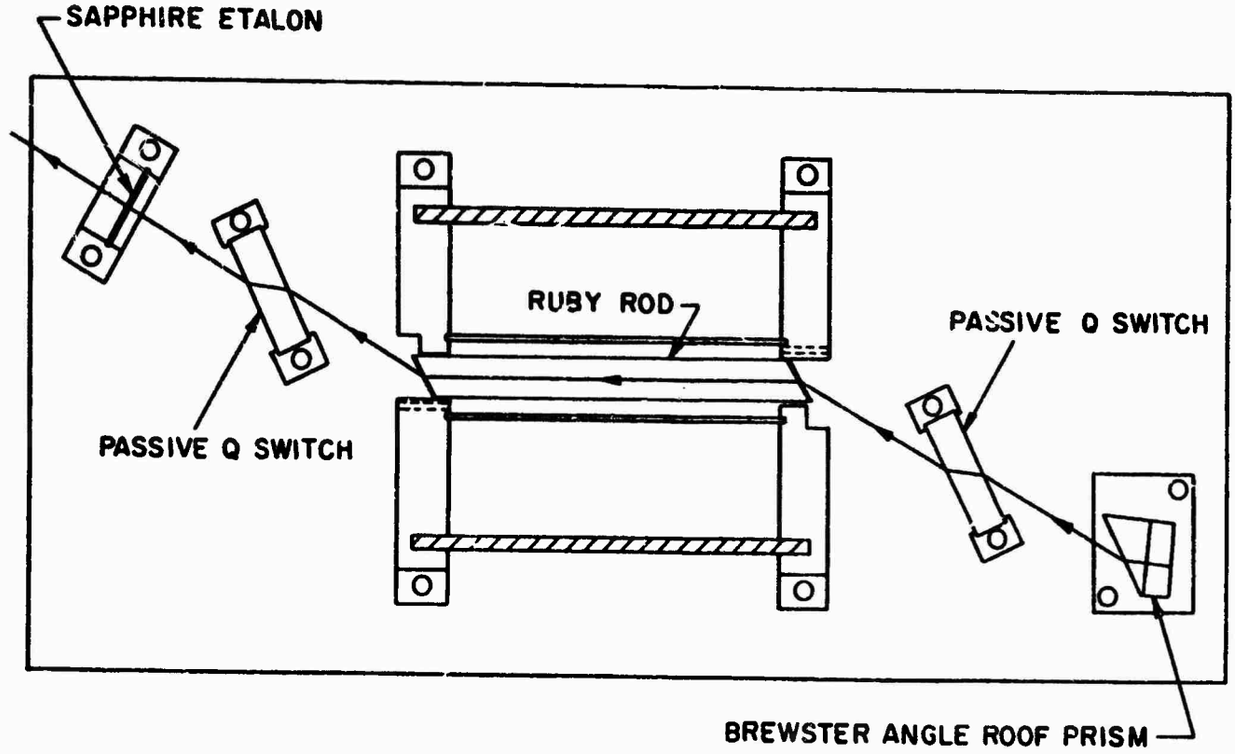

Figure IV-2a - Top view of high power ruby laser

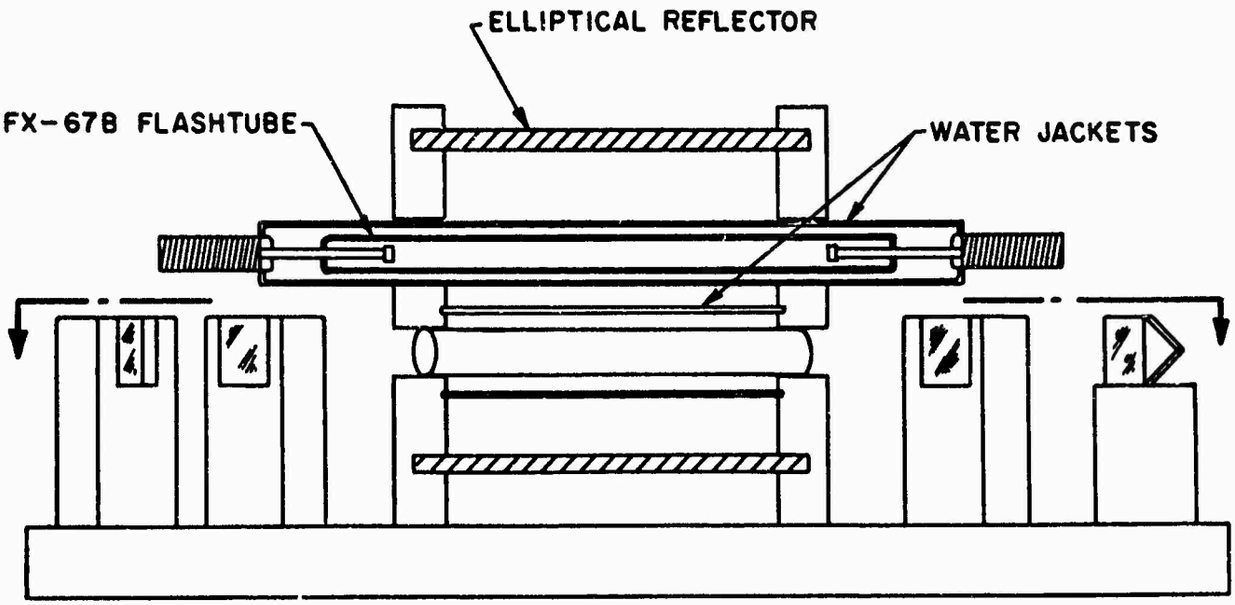

Figure IV-2b - Side view of high power ruby laser

SECTION V

INTERPRETATION OF RESULTS

In this section we consider some of the interpretation of the experimental results and examine some of the phenomena which play a role in these interactions. The main emphasis will be on a treatment of the expansion of a hot dense gas cloud and its subsequent cooling.

A. EXPANSION OF LASER PRODUCED MATERIAL

After a cloud of laser desorbed material is produced in front of the target in a vacuum environment it will expand. If the material is hot, the original thermal energy will be transformed into energy of expansion. By means of fairly simple equations we can determine the expansion of the gas and its cooling. The thermal energy appears at a distance from the interaction as an ordered energy of expansion. The velocities of the individual particles detected some distance away will correspond to energies higher than the thermal energies in the gas cloud.

Since these properties are characteristic of the actual emission that we observe experimentally, this model is appealing to examine in more detail. What follows is a simple derivation of the expansion of a cloud of hot blowoff material produced near a metal surface. The gas is considered as a continuum in thermal equilibrium, with the work done by the gas in expanding set equal to the increase in kinetic energy of expansion.

It should be emphasized that this work represents a beginning, not a complete model. This treatment is one dimensional. Radiation from the gas is neglected. The possibility of absorption of laser radiation in the blowoff material is not examined; it is merely assumed that the gas exists in a hot condition in front of the target at the end of the laser pulse. The possibility

of neating by absorption of laser radiation is allowed for by permitting the initial temperature to be an independent variable. The results of this treatment yield some characteristics in accord with experimentally observed properties, but before it can be considered as a description much additional work remains to be done.

We assume a one dimensional expansion, away from the surface. This condition is certainly not completely accurate, but it is supported by photographs of the plume of vaporized material, in which the expansion in a direction normal to the surface is much greater than the expansion in the transverse direction.

If A is the cross sectional area of the plume, X is the distance of the expanding edge from the surface, and N is the total number of molecules, and if we assume that the ideal gas law holds (as is likely since we expect relatively low particle densities) then the pressure P and temperature T are related by:

$$P = \frac{N k T}{AX} \tag{1}$$

This assumes a uniform distribution of molecules within the expanding gas cloud. This assumption is unrealistic. We will later modify this assumption, but for the present derivation, we assume that behind the expanding edge of the cloud, the density at a particular time does not vary with distance from the surface.

If we denote the velocity of the expanding edge by $\dot{X}$, the density at time t is $N/X(t)A$ and the density at time $t + \Delta t$ is $N/(X + \dot{X}\Delta t)A$. For a thin layer of gas at distance x from the surface, the outward velocity of the layer is denoted by dx/dt. The net change in density of molecules within the layer in time Δt is:

$$\left(\frac{d}{dx} \frac{N}{XA} \frac{dx}{dt} \Delta t \right)$$

and this must equal $\frac{N}{XA} - \frac{N}{(X + \dot{X}\Delta t)A}$

$$= \frac{N}{A} \frac{\dot{X}\Delta t}{(X^2 + X\dot{X}\Delta t)} \simeq \frac{N\dot{X}\Delta t}{A X^2} \left(1 - \frac{\dot{X}\Delta t}{X}\right)$$

$$\approx N\dot{X}\Delta t / A X^2$$

to first order in Δt. This leads to

$$\frac{1}{X} \frac{d}{dx} \frac{dx}{dt} = \frac{\dot{X}}{X^2}$$, with the boundary condition

$dx/dt = \dot{X}$ at $x = X$. We immediately obtain $\frac{dx}{dt} = \frac{x\dot{X}}{X}$. The energy of expansion in the material is then given by:

$$\frac{1}{2} \frac{N}{XA} M \int_0^X \left(\frac{\dot{X}x}{X}\right)^2 A\,dx = \frac{1}{6} NM \dot{X}^2$$

where M is the ion mass. The rate at which this energy changes is equal to the rate at which the gas cloud does work, or

$$P A \dot{X} = \frac{d}{dt} \frac{1}{6} NM \dot{X}^2 \qquad (2)$$

Finally, we equate the rate at which the gas cloud does work to the change in internal energy of the gas:

$$-\frac{d}{dt} \frac{1}{2} N k T = PA \dot{X} \qquad (3)$$

where we have again assumed ideal gas properties, and used the one dimensional nature of the problem. If we carry out the differentiation on the right hand side of (2) and substitute (1) on the left hand side, we obtain:

$$T = \frac{1}{3} \frac{M X}{k} \frac{d^2 X}{dt^2} \tag{4}$$

Consider now the expression:

$$\frac{d^3}{dt^3} (X^2) = \frac{d}{dt} \left[2 X \frac{d^2 X}{d t^2} + 2 \dot{X}^2 \right]$$

Using (4) and (2) on the right hand side of the above equation:

$$\frac{d^3 (X^2)}{d t^3} = \frac{d}{dt} \frac{6 k T}{M} + \frac{12 P A \dot{X}}{N M}$$

and then substituting (3) for dT/dt, we obtain

$$\frac{d^3 (X^2)}{dt^3} = 0 \tag{5}$$

To obtain boundary conditions for use with (5), we consider a laser pulse of duration t_p evaporating material from the surface at a temperature T_o. The end of the laser pulse is taken as $t = 0$. During the laser pulse, the material moves at the thermal velocity $(kT_o/M)^{1/2}$ and by the end of the pulse the edge of the cloud is at $X = (kT_o/M)^{1/2} t_p$. Thus at $t = 0$, $X = (kT_o/M)^{1/2} t_p$ $\dot{X} = (kT_o/M)^{1/2}$ and, using equation (4), $\ddot{X} = \frac{3}{t_p} \left(\frac{kT_o}{M} \right)^{1/2}$. Solving (5) using these boundary conditions gives

$$X = \left(\frac{kT_o}{M} \right)^{1/2} t_p \, (4t'^2 + 2t' + 1)^{1/2}$$

where $t' = t/t_p$. From this equation the motion of the expanding gas can be obtained easily as a function of time, as the thermal energy goes into directed energy of expansion.

Now let us remove the assumption of a uniform density. This assumption is somewhat unrealistic; we would expect that as the material moves out the density would be least at the expanding edge. If we assume that there is a linear density gradient, so that the particle density n is given by

$$n = n_s \, (1 - x/X) \tag{6}$$

where n_s is the particle density near the surface as a function of time, this situation is realized. While this approximation is doubtless not particularly accurate, it is physically more appealing than assuming a constant density behind the expanding edge.

With this assumption we can carry out a derivation similar to that described above for the constant density case. The reasoning is identical, but the equations become somewhat more complicated. We again obtain equation (5) for the position of the expanding edge, but the boundary conditions at $t = 0$ become

$$X = \left(\frac{kT_o}{M}\right)^{1/2} t_p \qquad \dot{X} = \left(\frac{k\,T_o}{M}\right)^{1/2}, \ddot{X} = \frac{6}{t_p}\left(\frac{k\,T_o}{M}\right)^{1/2}$$

Solving (5) using these boundary conditions yields the results:

$$X = \left(\frac{k\,T_o}{M}\right)^{1/2} t_p \quad (7\,t'^{2} + 2\,t' + 1) \tag{7}$$

The equation analogous to (4) becomes:

$$T = \frac{1}{6}\,\frac{M}{k}\,X\,\frac{d^2X}{dt^2} \tag{8}$$

The same result for the velocity of a shell of gas dx/dt at position X can be obtained as for the uniform density case:

$$\frac{dx}{dt} = \frac{x}{X}\,\dot{X} \tag{9}$$

We may use (7) and (8) to calculate the expansion and resulting cooling of the gas as functions of time. At a given distance from the surface, at a point which the edge of the gas cloud has passed, the flux is given by n dx/dt and it may be evaluated using equations (6) and (7).

We have not carried out the derivation of equations (6) - (9) in detail here, because the procedure becomes lengthy and tedious. All the reasoning required is demonstrated in the derivation for the uniform density case, and the form of the results is very similar.

Some results obtained using equations (6) - (9) to calculate the expansion and cooling of a gas cloud are shown in Table V-1 and in Figure V-1. Table V-1 shows calculated results for the temperature and position of the expanding edge

TABLE V-1

CALCULATED EXPANSION AND COOLING OF GAS CLOUD

Time After End of Laser Pulse (Micro-seconds)	Position of Expanding Edge (cm)	Particle Energy (ev)	Temperature (°K)	
0	0.004	0.22	5000	Mass 28
0.03	0.012	1.38	500	
0.06	0.021	1.47	152	
0.09	0.030	1.49	71	
0.12	0.040	1.50	41	
0.30	0.098	1.51	6.9	
0.60	0.194	1.51	1.7	Initial Temperature
0.90	0.291	1.51	0.7	
1.5	0.483	1.51	0.2	5000°K
3.0	0.966	1.51	0.0	
0	0.005	0.43	10000	Mass 28
0.03	0.016	2.76	1000	
0.06	0.030	2.94	303	
0.09	0.043	2.98	143	
0.12	0.057	3.00	83	
0.30	0.138	3.02	13.8	
0.60	0.275	3.02	3.5	Initial Temperature
0.90	0.411	3.02	1.5	
1.5	0.684	3.02	0.5	
3.0	1.366	3.02	0.1	10,000°K
0	0.012	2.16	50000	Mass 28
0.03	0.036	13.80	5000	
0.06	0.066	14.70	1515	
0.09	0.096	14.91	714	
0.12	0.127	14.99	413	
0.30	0.309	15.08	69	
0.60	0.614	15.09	17.5	Initial Temperature
0.90	0.919	15.09	7.8	
1.5	1.529	15.09	2.8	
3.0	3.053	15.09	0.7	50,000°K

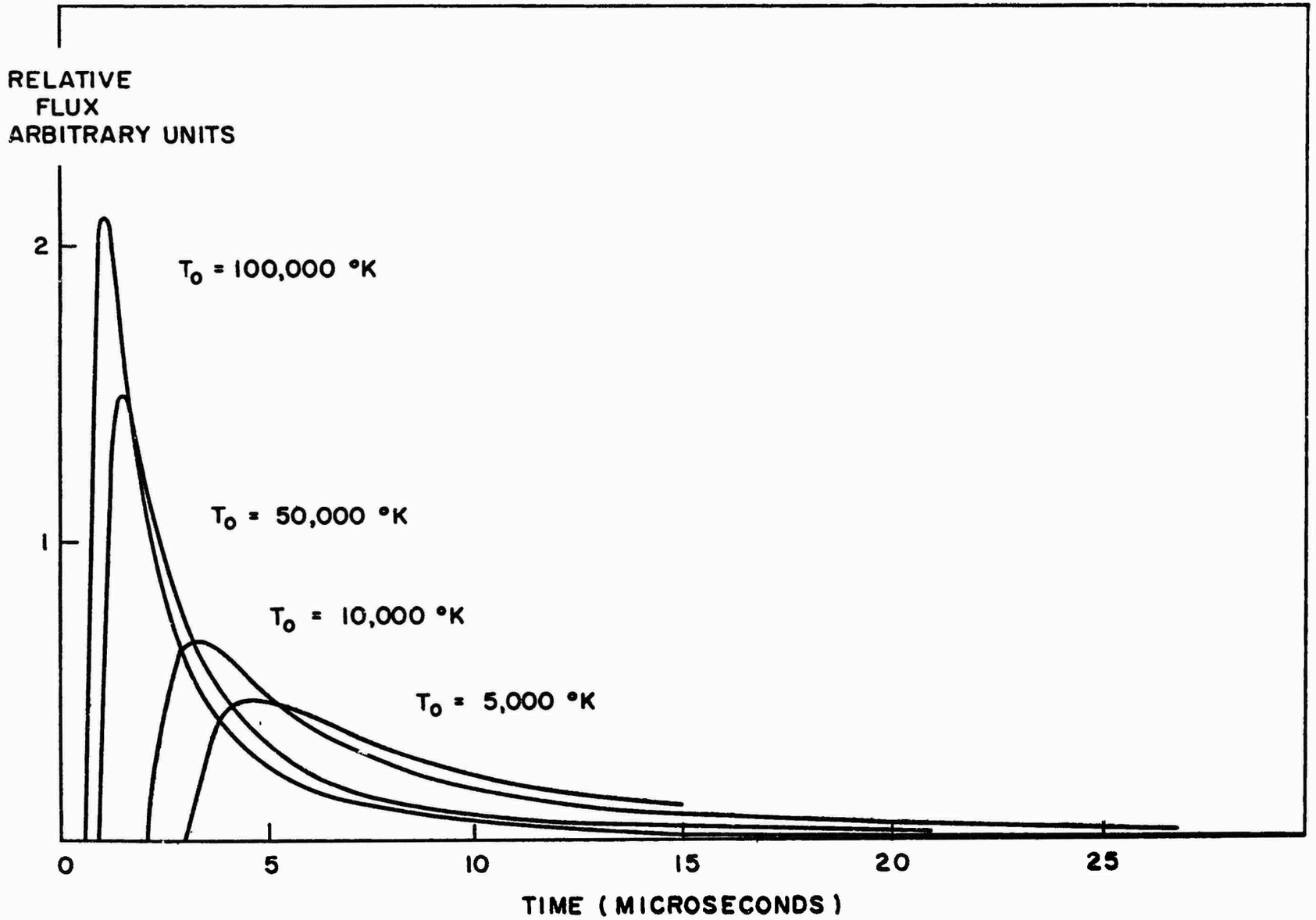

Figure V-1 - Calculated particle fluxes as a function of time at a position one centimeter from the surface for mass 28 molecules at various initial temperatures.

the surface for mass 28 molecules at various initial temperatures.

for a gas of mass 28 amu at various times after the end of the laser pulse, for different values of the assumed initial temperature T_o. A value of T_o equal to 5000°K would correspond to material desorbed from a hot but not vaporized tungsten surface with no subsequent heating of the gas. A value of 50,000°K would involve considerable heating after the gas had left the surface. Table V-1 also lists particle energies corresponding to the energy of a mass 28 amu molecule traveling at the velocity of the edge of the gas cloud. It is apparent how the particle energy increases as the gas cools. These particle energies are greater than the original thermal energy of a molecule in the gas. They represent an ordered motion of the gas moving out from the surface. It is apparent that the gas cools very rapidly, giving up almost all its thermal energy in a few hundred nanoseconds. Thereafter, the expansion proceeds at an essentially constant rate and the particle energy is constant.

Quantitatively these results are similar to the experimental results for ion pulses, i.e., an ordered motion of expansion with a smaller thermal component. However, even for T_o equal to 50,000°K, the energies are still much smaller than those found experimentally.

Figure V-1 shows relative particle fluxes as a function of time at a distance one centimeter from the surface. These results were calculated using equations (6) and (9). The pulse shapes are similar to those produced by the high energy neutral molecules and by the high energy ions. Of course, to get a realistic comparison, the much greater distance of flight in the experimental apparatus must be considered, and for the ions, the effect of an accelerating voltage must be included. However, the similarity is very striking. Comparison of pulse shapes calculated for a detector placed a greater distance from the surface may provide a way of deducing initial conditions in the gas.

In summary, the work described above offers some insight into the behavior of the laser produced gas, and some features appear similar enough to experimental results to warrant further work although calculated particle energies are low. In this further work, the model must be refined, and such effects as absorption of laser light in the gas, radiation from the gas, and the possible effect of electrostatic forces in accelerating ions must be included.

The picture deduced from this analysis is consistent with the high energy neutral molecule and ion pulses being produced by expansion of a heated gas cloud, provided that the desorbed gas can be heated very hot during the laser pulse. The heating extrapolating the results of Table V-1 would have to be to a temperature of about 500,000°K. This would lead to energies of expansion with superposed random components of the same order of magnitude as we observe in the time-of-flight spectrometer.[3] However, a mechanism capable of providing this heating is unknown. Our earlier work[2] on heating by inverse Bremsstrahlung indicates that in our experimental conditions, that mechanism would not be likely to provide sufficient heating. Clearly, this picture has appealing features, but needs considerably more analysis.

B. VELOCITY DISTRIBUTIONS

Previously, we calculated ion velocity distributions from the measured pulse shapes using a method suggested by F. J. Allen[3]. An attempt was then made to fit the calculated distributions to a maxwellian of the form:

$$N(w_X) = N \left(\frac{M}{2\pi k T}\right)^{1/2} \exp\left[-\frac{M}{2kT}\left(w_X - \bar{w}_X\right)^2\right] \qquad (1)$$

where all quantities are defined in ref. 3. It has since been pointed out by Allen that if one assumes a maxwellian distribution superimposed on a directed component of velocity normal to the target, the correct form of the maxwellian seen at the end of the drift tube is, for small solid angles,

$$N(w_X) = N\left(\frac{M}{2\pi k T}\right)^{3/2} \pi \left(\frac{a v_d}{\ell}\right)^2 \exp\left[-\frac{M}{2 k T}(w_X - \bar{w}_X)^2\right] \quad (2)$$

with all variables as defined in Ref. 3.

He also pointed out that because of the weak dependence of v_d on w_X, no great difference should be expected between the pulse shapes obtained from (1) and (2).

We have tried to fit the pulse shapes shown in Figures III-2 and III-3 of an earlier report [3] using the maxwellian of equation (2). Figures V-2 and V-3 show the actual velocity distribution, labeled data, for ions of mass 39 and 23 respectively; also shown are maxwellian fits to the data using equations (1) and (2), which are labelled "old maxwellian" and "new maxwellian", respectively. It can be seen that the results obtained using either (1) or (2) are essentially identical.

The interest in this particular point derives from the fact that there are persistent differences in the shape of the experimentally determined velocity distribution and the maxwellian distribution calculated from (1). The development of equation (2) was an attempt to improve the agreement of experimental and calculated curves by a more proper formulation of the maxwellian, but the use of equation (2) does not improve the fit.

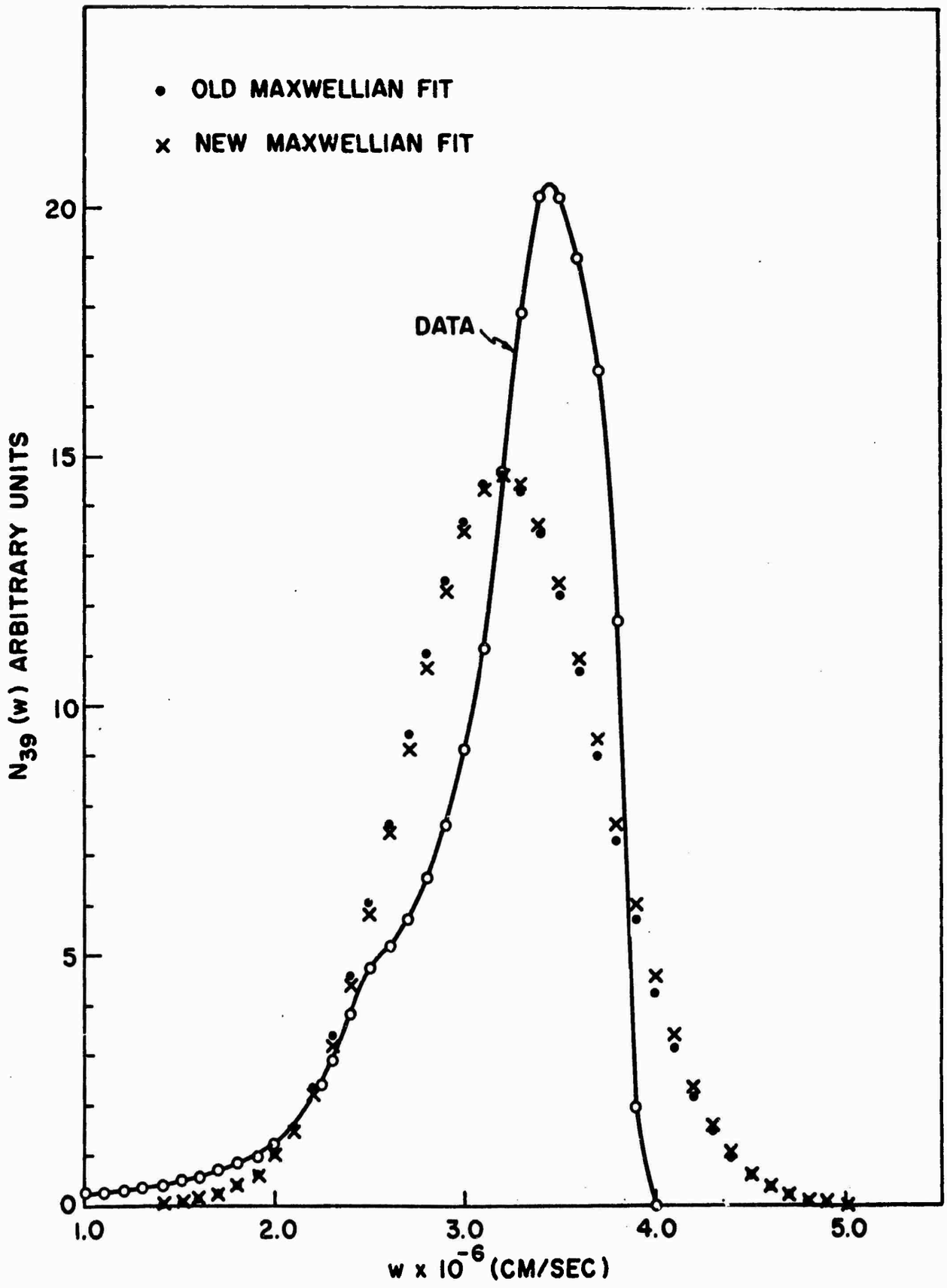

Figure V-2 - Velocity distribution and calculated maxwellian distributions for mass 39 ions.

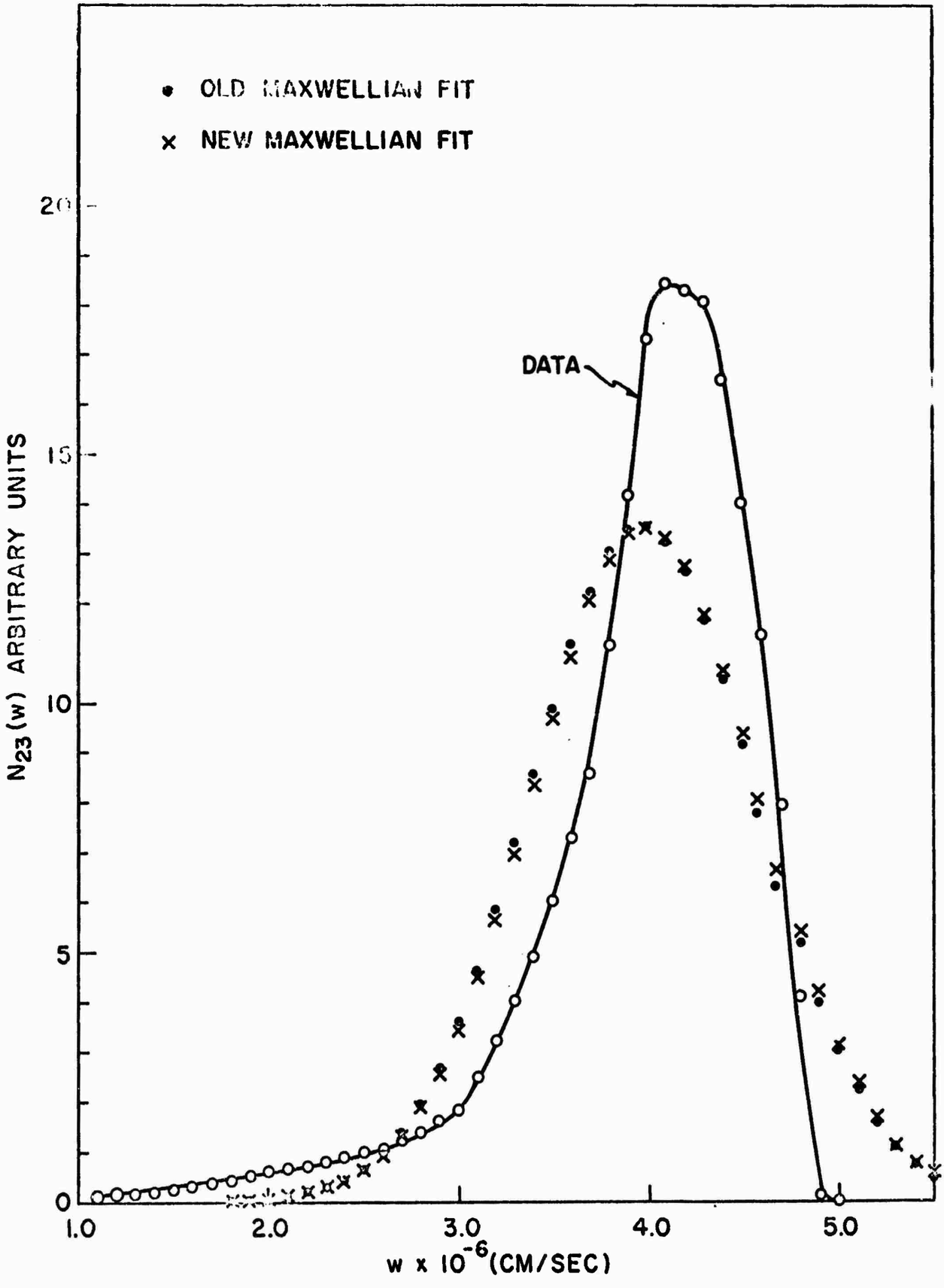

Figure V-3 - Velocity distribution and calculated maxwellian distributions for mass 23 ions.

C. CALCULATION OF ION PULSE SHAPES FROM INFERRED VELOCITY DISTRIBUTIONS

In a previous report [3] we had calculated the shapes of ions pulses arriving at the detector following the drift tube in the time-of-flight spectrometer. Most of the work was done using the assumption that the emission occurs as a delta function in time. In an attempt to see if this restriction could be removed, some calculations were made for the pulse shapes using the assumption that the emission occurs as a square pulse in time and that the velocity distribution is maxwellian. Using the notation of reference (4), this leads to an ion current J(t) as a function of time t at a fixed position X:

$$J(t) = \int_{w_{min}(t)}^{w_{max}(t)} A\,[t - \tau(X,w)] \left[\frac{M}{2\pi k T (t-\tau)}\right]^{1/2} \exp\left[\frac{M w^2}{2 k T (t-\tau)}\right] dw \quad (1)$$

where A(t) is the temporal shape of the emission pulse, and

$$\tau(X,w) = \int_0^X \frac{dX}{v(X,w)}$$

In Section III. A. 3 of reference (4) we described the numerical evaluation of J(t) for various assumptions about the temperature of emission and the shape of the emission pulse. Results of that section indicated that the calculated pulse shape was not particularly sensitive to variation of the available parameters, so long as a maxwellian velocity distribution is assumed. These pulse shapes moreover did not agree particularly well with the pulse shapes calculated using a delta function approximation. The pulse shapes calculated on the delta function approximation rose steeply to a peak value and fell off more slowly, whereas the pulse shapes calculated using equation (1) above with a square emission pulse were more symmetric.

Additional work has been performed on evaluating equation (1) for some further choices of input parameters, in particular for a relatively long emission time and relatively low temperature of emission.

Figure V-4 shows the results of numerically evaluating equation (1) for mass 39 ions with 1000 volts accelerating potential, and an assumed triangular emission pulse shape of one microsecond duration and a maxwellian distribution corresponding to a temperature of 10^4°K. The results shown here are very similar in pulse shape to the results shown in curve 3 of Figure III-11 of reference (3), which was obtained assuming a non-maxwellian velocity distribution with a delta function emission pulse. The times of arrival and pulse lengths are not identical for these two curves but this can be adjusted by choice of the emission pulse shape; it is the ability to reproduce, at least approximately, the shape of the pulse that is important in the present argument.

Thus, results of calculations such as these cannot distinguish uniquely between different possible sets of conditions on initial pulse shapes and distributions. This confirms that one cannot work back from observed ion pulse shapes to a complete specification of initial conditions; this problem is underdetermined.

The additional work described in this subsection essentially completes the work described in Section III. A. 3 of reference (3). While the result is essentially negative, in that it shows that the original emission characteristics cannot be completely determined from the shape of the ion current pulse, it does rule out many plausible combinations for these conditions. Thus according to the work described in Ref. 3, an emission pulse lasting several hundred nanoseconds and characterized by a maxwellian velocity distribution is eliminated. We must either assume very long (about one microsecond) durations for the emission, a not very appealing choice, or assume non-maxwellian velocity distributions.

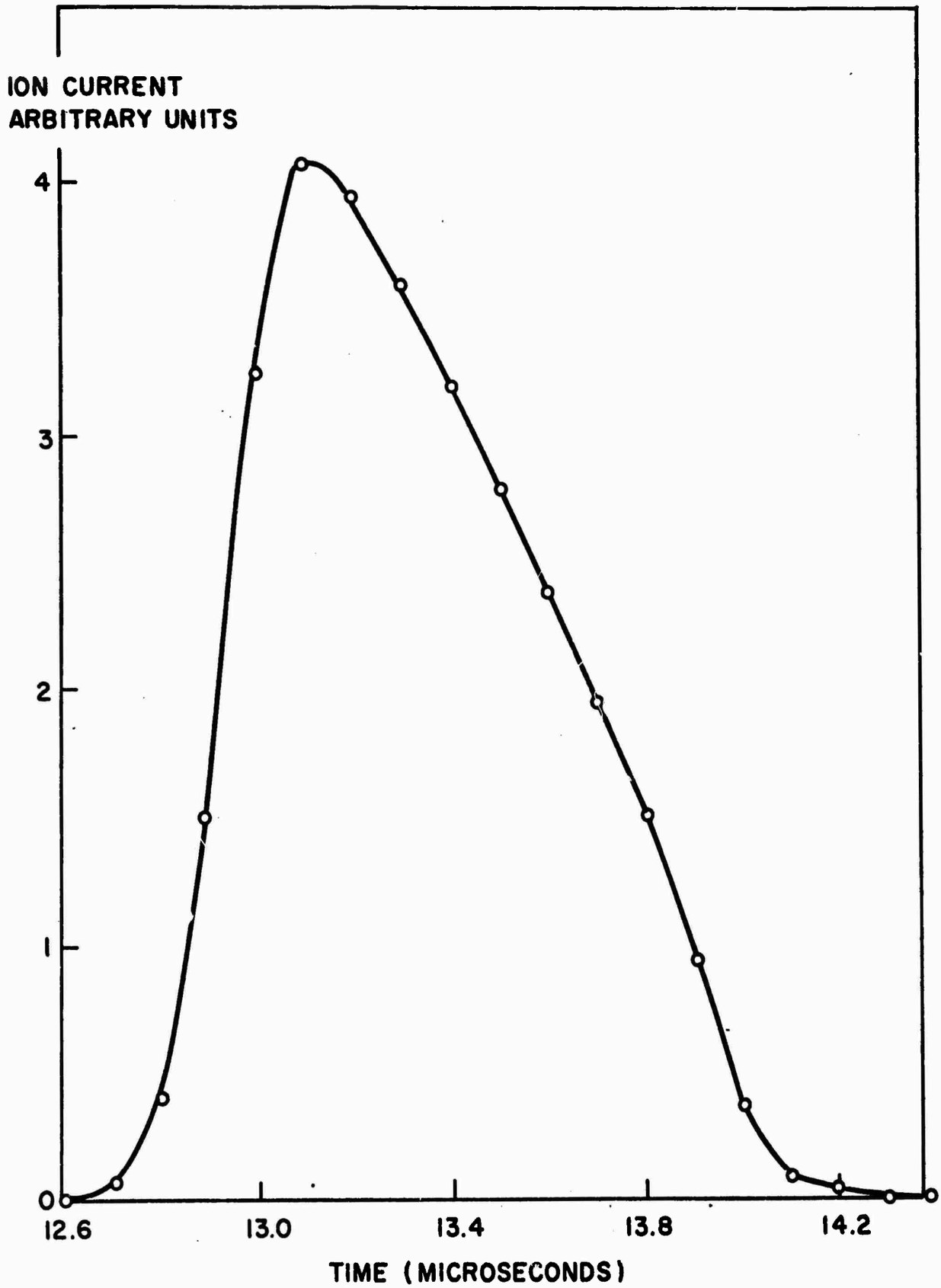

Figure V-4 - Calculated ion pulse shape for mass 39 ions, 1000 volt accelerating potential, 10^4 °K maxwellian velocity distribution, and one microsecond triangular emission pulse.

D. INVERSE BREMSSTRAHLUNG

In earlier reports [2, 3] we described calculations that indicated that absorption of the laser light in the blowoff material by the inverse Bremsstrahlung process in the field of an ion does not produce significant heating of the blowoff material under our experimental conditions. This process, however, could be expected to produce heating under conditions of higher laser power.

Interest in heating the blowoff material is spurred by the velocity distribution analysis of our ion pulses [3] and by the discussion in Section V. A. These two things taken together indicate that our results are compatible with a relatively modest heating, of the order of 30 ev, followed by expansion of the hot material.

We had suggested [3] that even though charged particle densities are too low to permit appreciable inverse Bremsstrahlung absorption in the fields of ions, still there might be significant absorption by the same process in the neighborhood of neutral atoms and molecules. For our experimental situation, where we observe large pulses of neutral gases, such as CO, we might expect relatively large densities of neutral molecules near the surface during the laser pulse. The densities could be as high as 10^{18} neutral molecules/cm^3. Even though the cross section for absorption near a neutral molecule would be much lower than for an ion, we felt this process would be worth considering because of the relatively high densities of neutral particles. Accordingly, we devoted some effort toward an attempt to estimate the absorption cross section for molecules such as CO. This problem is very difficult and requires a complete quantum mechanical formulation. It rapidly appeared that any realistic solution that took into account the structure of the CO molecule would be an extremely large problem and outside the scope of this contract.

Accordingly, we have made use of an expression[10] derived for absorption of light by an electron near a hydrogen molecule. This doubtless is not accurate for other neutral molecules, but should indicate orders of magnitude. The absorption cross section per hydrogen molecule, for ruby laser light, is given by:

$$[\ 7.7 + 79.9/\theta\ -\ 19.0/\theta^2]\ x\ 10^{-41} n_e \quad cm^2$$

where n_e is the electron density and $\theta = 5040/T$ with T the temperature of the medium. For a temperature of a few thousand degrees, a neutral molecule density of $10^{18}/cm^3$, and an electron density of $10^{13}/cm^2$ this leads to an absorption coefficient of the order of 10^{-8} per cm in the material. If we denote by I_o the total energy per unit area in the laser pulse, the total energy absorbed per molecule is about:

$$10^{-8}\ I_o/n$$

where n is the neutral molecule density. We have $I_o \approx 2\ j/cm^2$ which leads to a calculated energy absorption of the order of 10^{-7} ev per neutral molecule. The energy is actually absorbed by electrons, but for heating the energy must be shared among the molecules; this effect can produce virtually no heating.

The conclusion is that absorption by the inverse Bremsstrahlung process in the field of neutral molecules is not a likely process for producing a hot gas. Neither was the same interaction in the field of ions, for our experimental conditions. Thus, we have no convincing mechanism at present for transfer of energy from the laser beam to the blowoff material.

SECTION VI

CONCLUSIONS

In this report we have described measurements on laser produced ion emission in the time-of-flight spectrometer and neutral particle emission in the quadrupole spectrometer. This work extends similar studies using the same equipment. The main features of the emission are similar to those reported before. The emphasis on this report is on details, such as the differences in emission between different target materials and the dependence of the emission on laser power. The work has also involved new target materials, notably carbon and nickel.

Ion emission from carbon targets includes $(Li^6)^+$, $(Li^7)^+$, C^+, CH_3^+, H_2O^+, Na^+ and K^+ ions. The energies of the alkali ions in this list range up to 540 ev, higher than values obtained earlier from tungsten and platinum targets. The ion emission from single crystalline nickel targets is broadly similar to that from tungsten and platinum. The range of energies is somewhat higher, up to 360 ev. We have also seen evidence of Na^{++} and H_2^+ emitted from the nickel. These are species not previously observed in this work. The hydrogen emission became noticeable only after the target had been heated with the system backfilled with hydrogen. In addition, we have seen nickel ions.

Because of apparently anomalous results on the high energy neutral molecule pulses from titanium, we rechecked some previous work on tungsten targets. During the course of this work, we investigated the influence of spectrometer condition on these pulses, and found that if the spectrometer were not tuned opaque with ionization chamber grids grounded, spurious results could arise. These spurious effects had caused the anomalous results from titanium.

During this work we also checked and reconfirmed our earlier conclusions on the nature of the high energy neutral molecule pulses.

Measurements using this system were extended to carbon targets. The high energy neutral molecule pulses from the different materials display distinctive features. For example, titanium displays a pulse (apparently hydrogen) which disappears upon heating; while carbon targets never emit a pulse that arrives early enough to be identified as hydrogen. Some evidence was obtained that the high energy neutral molecules may be H_2, CO, and CO_2, but the identification is not certain. We have also obtained information on how the arrival times (and thus the energies) of the high energy neutral molecules vary over a large range of incident laser powers. Energies of the order of 100 ev are typical.

We have also described the construction of apparatus for other types of measurements, in particular a high power (100 megawatt) ruby laser, and equipment for measurement of the angular distribution of ions and for measurement of energies of electrons produced in the laser-surface interaction.

Finally, we discussed a model in which a hot gas expands, converting its thermal energy into an ordered energy of expansion. The treatment to date is simple and requires additional work, but the calculated pulse shapes are similar to those observed in the high energy neutral molecule and ion emission experiments. The results indicated particle energies at the expanding front higher than the thermal energy in the original gas cloud. This is similar to the results obtained for ion velocity distributions from analysis of ion pulse shapes. We lack, however, a plausible mechanism to explain heating of the original gas cloud to the required high temperature.

REFERENCES

1. "Mechanisms of Laser-Surface Interactions", by J. F. Ready, E. Bernal G., L. P. Levine, Final Report to Ballistic Research Laboratories on Contract DA-11-022-AMC-1749 (A), March 1965.

2. IBID. Semi-Annual Report on Contract DA-11-022-1749 (A) Mod 2, November 1965.

3. IBID. Final Report on Contract DA-11-022-AMC-1749 (A) Mod. 2, May 1966.

4. Supplied by the High Temperature Materials, Inc., Lowell, Mass. through the courtesy of Mr. Phillip Higgs.

5. See, for example, Handbook of Chemistry and Physics, 42nd Ed., Chemical Rubber Publishing Co., Cleveland, Ohio (1961).

6. D. Lichtman, Private Communication.

7. L. H. Germer, talk given at Honeywell Corporate Research Center, Hopkins, Minnesota (1965).

8. F. Floux, P. Langer, G. Tonon, "Laser Induced Emission of Electrons, Ions and X-rays." Paper presented at the Fourth Quantum Electronics Conference, Phoenix, Arizona, April 1966.

9. "Production of Plasmas for Thermonuclear Fusion by Laser Beam Irradiation of Solid Particles", by A. F. Haught and D. H. Polk, Quarterly Report to AEC on Contract AT(30-1)-3578, March 1966.

10. W. B. Sommerville, Astrophysical Journal 139, 192 (1964).

Unclassified
Security Classification

DOCUMENT CONTROL DATA - R&D

(Security classification of title, body of abstract and indexing annotation must be entered when the overall report is classified)

1. ORIGINATING ACTIVITY (Corporate author)	2a. REPORT SECURITY CLASSIFICATION
Honeywell Inc. Corporate Research Center Hopkins, Minnesota	Unclassified 2b GROUP

3. REPORT TITLE

MECHANISMS OF LASER-SURFACE INTERACTIONS

4. DESCRIPTIVE NOTES (Type of report and inclusive dates)

Semi-Annual Report,

5. AUTHOR(S) (Last name, first name, initial)

Ready, J. F. and Bernal G., E.

6. REPORT DATE	7a. TOTAL NO. OF PAGES	7b. NO. OF REFS
December 1966	85	10

8a. CONTRACT OR GRANT NO.	9a. ORIGINATOR'S REPORT NUMBER(S)
DA-18-001-AMC-1040(X) b. PROJECT NO. c. d.	9b. OTHER REPORT NO(S) (Any other numbers that may be assigned this report)

10. AVAILABILITY/LIMITATION NOTICES

Distribution of this document is unlimited.

11. SUPPLEMENTARY NOTES	12. SPONSORING MILITARY ACTIVITY
	U.S. Army Ballistic Research Laboratories Aberdeen Proving Ground, Maryland

13. ABSTRACT

This report extends earlier measurements on particle emission produced when approximately 50 megawatts/cm^2 pulses of radiation from a Q-switched ruby laser are absorbed at metal surfaces. Ion emission from carbon targets includes $(Li^6)^+$, $(Li^7)^+$, C^+, CH_3^+, H_2O^+, Na^+, and K^+ ions with energies up to 540 ev. Emission from single crystalline nickel targets includes ion species not observed before in this work, i.e., Na^{++} and H_2^+. Work using a quadrupole mass spectrometer to study neutral molecule emission has also been extended to carbon targets, which yield results similar to other target materials, and additional confirming work on the presence of high energy neutral molecules has been performed. Equipment under construction for measurement of the angular distribution of the ion emission is described. The expansion of the laser produced gas and resulting particle fluxes at a distance from the surface are discussed.

DD FORM 1 JAN 64 1473

Unclassified
Security Classification

14. KEY WORDS	LINK A		LINK B		LINK C	
	ROLE	WT	ROLE	WT	ROLE	WT
Laser Plasma Mass Spectrometry Desorption						

INSTRUCTIONS

1. ORIGINATING ACTIVITY: Enter the name and address of the contractor, subcontractor, grantee, Department of Defense activity or other organization *(corporate author)* issuing the report.

2a. REPORT SECURITY CLASSIFICATION: Enter the overall security classification of the report. Indicate whether "Restricted Data" is included. Marking is to be in accordance with appropriate security regulations.

2b. GROUP: Automatic downgrading is specified in DoD Directive 5200.10 and Armed Forces Industrial Manual. Enter the group number. Also, when applicable, show that optional markings have been used for Group 3 and Group 4 as authorized.

3. REPORT TITLE: Enter the complete report title in all capital letters. Titles in all cases should be unclassified. If a meaningful title cannot be selected without classification, show title classification in all capitals in parenthesis immediately following the title.

4. DESCRIPTIVE NOTES: If appropriate, enter the type of report, e.g., interim, progress, summary, annual, or final. Give the inclusive dates when a specific reporting period is covered.

5. AUTHOR(S): Enter the name(s) of author(s) as shown on or in the report. Enter last name, first name, middle initial. If military, show rank and branch of service. The name of the principal author is an absolute minimum requirement.

6. REPORT DATE: Enter the date of the report as day, month, year; or month, year. If more than one date appears on the report, use date of publication.

7a. TOTAL NUMBER OF PAGES: The total page count should follow normal pagination procedures, i.e., enter the number of pages containing information.

7b. NUMBER OF REFERENCES: Enter the total number of references cited in the report.

8a. CONTRACT OR GRANT NUMBER: If appropriate, enter the applicable number of the contract or grant under which the report was written.

8b, 8c, & 8d. PROJECT NUMBER: Enter the appropriate military department identification, such as project number, subproject number, system numbers, task number, etc.

9a. ORIGINATOR'S REPORT NUMBER(S): Enter the official report number by which the document will be identified and controlled by the originating activity. This number must be unique to this report.

9b. OTHER REPORT NUMBER(S): If the report has been assigned any other report numbers *(either by the originator or by the sponsor)*, also enter this number(s).

10. AVAILABILITY/LIMITATION NOTICES: Enter any limitations on further dissemination of the report, other than those imposed by security classification, using standard statements such as:

(1) "Qualified requesters may obtain copies of this report from DDC."

(2) "Foreign announcement and dissemination of this report by DDC is not authorized."

(3) "U. S. Government agencies may obtain copies of this report directly from DDC. Other qualified DDC users shall request through _____."

(4) "U. S. military agencies may obtain copies of this report directly from DDC. Other qualified users shall request through _____."

(5) "All distribution of this report is controlled. Qualified DDC users shall request through _____."

If the report has been furnished to the Office of Technical Services, Department of Commerce, for sale to the public, indicate this fact and enter the price, if known.

11. SUPPLEMENTARY NOTES: Use for additional explanatory notes.

12. SPONSORING MILITARY ACTIVITY: Enter the name of the departmental project office or laboratory sponsoring *(paying for)* the research and development. Include address.

13. ABSTRACT: Enter an abstract giving a brief and factual summary of the document indicative of the report, even though it may also appear elsewhere in the body of the technical report. If additional space is required, a continuation sheet shall be attached.

It is highly desirable that the abstract of classified reports be unclassified. Each paragraph of the abstract shall end with an indication of the military security classification of the information in the paragraph, represented as *(TS)*, *(S)*, *(C)*, or *(U)*.

There is no limitation on the length of the abstract. However, the suggested length is from 150 to 225 words.

14. KEY WORDS: Key words are technically meaningful terms or short phrases that characterize a report and may be used as index entries for cataloging the report. Key words must be selected so that no security classification is required. Identifiers, such as equipment model designation, trade name, military project code name, geographic location, may be used as key words but will be followed by an indication of technical context. The assignment of links, rules, and weights is optional.